Inorganic Chemistry

Article

pubs.acs.org/IC

# Tuning Electronic Structure, Redox, and Photophysical Properties in Asymmetric NIR-Absorbing Organometallic BODIPYs

Yuriy V. Zatsikha,[†,‡] Eranda Maligaspe,[†] Anatolii A. Purchel,[†] Natalia O. Didukh,[‡] Yefeng Wang,[¶] Yuriy P. Kovtun,[*,‡] David A. Blank,[*,¶] and Victor N. Nemykin[*,†]

[†]Department of Chemistry & Biochemistry, University of Minnesota Duluth, Duluth, Minnesota 55812, United States

[‡]Institute of Organic Chemistry, National Academy of Sciences of Ukraine, 5 Murmanska Strasse, 02660 Kyiv, Ukraine

[¶]Department of Chemistry, University of Minnesota, 207 Pleasant Street Southeast, Minneapolis, Minnesota 55455, United States

Supporting Information

**ABSTRACT:** Stepwise modification of the methyl groups at the $\alpha$ positions of BODIPY **1** was used for preparation of a series of mono- (**2**, **4**, and **6**) and diferrocene (**3**) substituted donor–acceptor dyads in which the organometallic substituents are fully conjugated with the BODIPY $\pi$ system. All donor–acceptor complexes have strong absorption in the NIR region and quenched steady-state fluorescence, which can be partially restored upon oxidation of organometallic group(s). X-ray crystallography of complexes **2**–**4** and **6** confirms the nearly coplanar arrangement of the ferrocene groups and the BODIPY $\pi$ system. Redox properties of the target systems were studied using cyclic voltammetry (CV) and differential pulse voltammetry (DPV). It was found that the first oxidation process in all dyads is ferrocene centered, while the separation between the first and the second ferrocene-centered oxidation potentials in diferrocenyl-containing dyad **3** is ∼150 mV. The density functional theory-polarized continuum model (DFT-PCM) and time-dependent (TD) DFT-PCM methods were used to investigate the electronic structure as well as explain the UV–vis and redox properties of organometallic compounds **2**–**4** and **6**. TDDFT calculations allow for assignment of the charge-transfer and $\pi \rightarrow \pi^*$ transitions in the target compounds. The excited state dynamics of the parent BODIPY **1** and dyads **2**–**4** and **6** were investigated using time-resolved transient spectroscopy. In all organometallic dyads **2**–**4** and **6** the initially excited state is rapidly quenched by electron transfer from the ferrocene ligand. The lifetime of the charge-separated state was found to be between 136 and 260 ps and demonstrates a systematic dependence on the electronic structure and geometry of BODIPYs **2**–**4** and **6**.

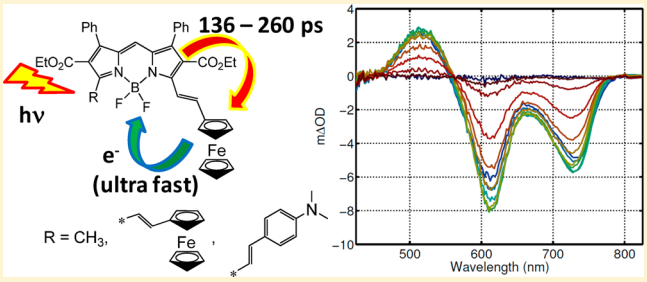


## INTRODUCTION

Light-induced charge separation is a key to the conversion of solar energy to electricity.[1] Efficient transformation of sunlight to electricity depends on many factors, including the absorption cross-section and spectral coverage, rate of electron transfer, excited state relaxation dynamics, and stability of the charge-separated (CS) state.[2] Not surprisingly, numerous donor–acceptor (D–A) dyads and donor–antennae–acceptor (D–An–A) triads have been extensively studied as possible candidates for solar energy conversion in artificial photosynthetic systems.[3] The electronic coupling between the donor and the acceptor in D–A and D–An–A systems depends on donor–acceptor spatial orientation and separation and the nature of the bridge between them.[3,4] For instance, formation of an exceptionally long-lived (230 $\mu$s) CS state was observed in a system with a relatively short, ∼2.6 Å, D–A distance.[5a]

Ferrocene derivatives can be used as efficient and robust electron donors in D–A assemblies. Numerous ferrocene-containing porphyrins,[6−10] tetraazaporphyrins,[11] phthalocyanines,[12] corroles,[13] and subphthalocyanines[14] have been intensively studied in conjunction with their exciting electron-transfer properties. More recently, non-macrocyclic 4,4-difluoro-4-bora-3a,4a-diaza-s-indacene (BODIPY)[15] and aza-BODIPY[16] platforms were also used in preparation of the ferrocene-containing D–A and D–An–A assemblies. As expected, in the case of ferrocene-containing BODIPYs and azaBODIPYs in which the organometallic group is not conjugated with the $\pi$ system of the BODIPY or azaBODIPY, the optical and redox properties are a superposition of the donor and antennae fragments.[15f−h] In the case of BODIPYs and azaBODIPYs, with ferrocene groups conjugated into the parent $\pi$ system, low-energy metal-to-ligand charge-transfer (MLCT) bands are commonly observed in the near-infrared (NIR) spectral region that are easily tunable in energy and intensity as was shown for alkynylferrocene-substituted BODIPYs.[15a−e] Examples of the ferrocene-containing BODIPYs with organometallic groups conjugated into the $\pi$ system

**Received:** May 1, 2015
**Published:** July 29, 2015




DOI: 10.1021/acs.inorgchem.5b00992
*Inorg. Chem.* 2015, 54, 7915–7928

**Scheme 1. Synthetic Pathways for Preparation of Organometallic BODIPYs 2−4 and 6**

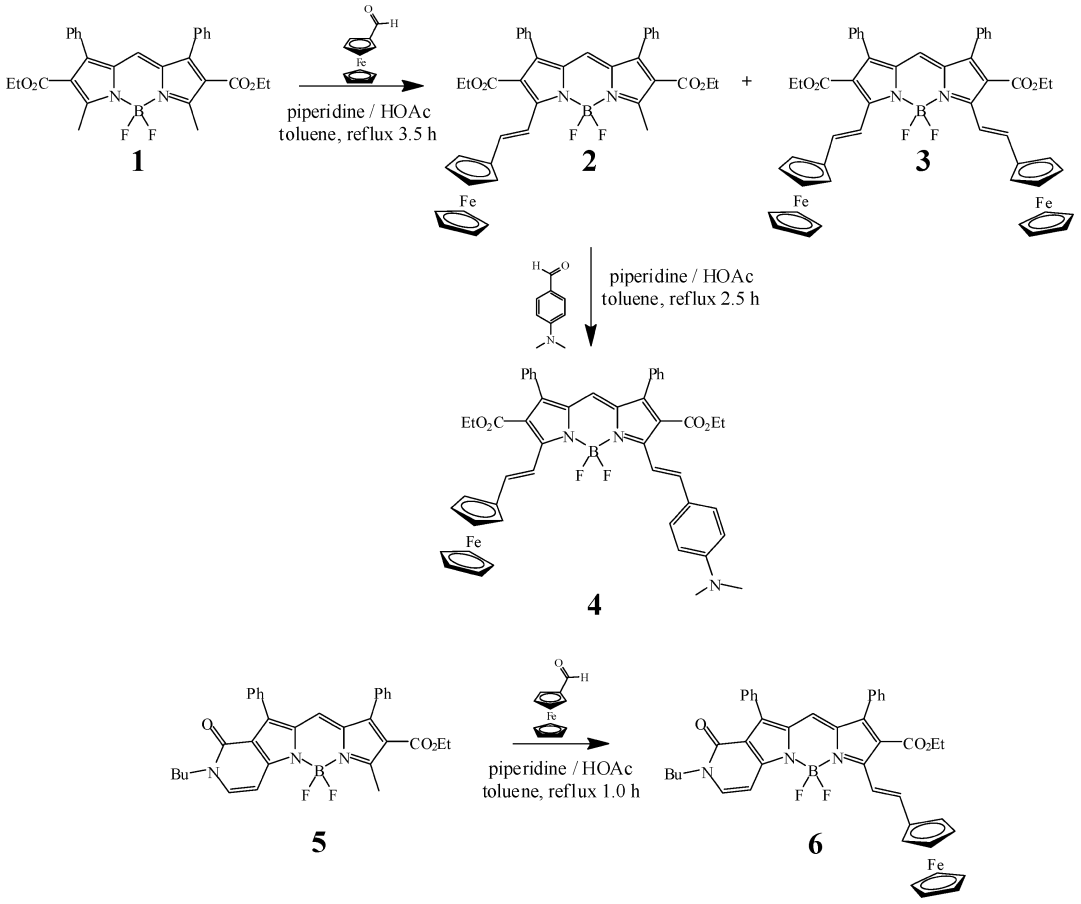


via vinyl bridging groups are rare, and no systematic study is available on the influence of the different substituents on the optical and redox properties of these systems.[15i,j] Thus, in this report, we discuss the preparation, redox, and photophysical properties of several symmetric and asymmetric ferrocene-containing D−A assemblies (Scheme 1) with strong absorption in the NIR region in which organometallic substituents are conjugated into the $\pi$ system via a vinyl bridge. The choice of BODIPYs was as follows: BODIPY **2** was chosen as a parent platform, BODIPYs **3** and **4** have an additional organometallic (**3**) or organic (**4**) electron-donating group, and BODIPY **6** has an additional electron-withdrawing group (Scheme 1).

## EXPERIMENTAL SECTION

**Reagents and Materials.** Solvents were purified using standard approaches: toluene was dried over sodium metal, THF was dried over sodium−potassium alloy, and hexane and DCM were dried over calcium hydride. Dimethyl BODIPY derivative **1**[17] and pyridone BODIPY derivative **5**[18] were prepared as described earlier. Silica gel (60 Å, 60−100 $\mu$m) was purchased from Dynamic Adsorbents Inc.

**Synthesis.** *1,7-Diphenyl-2,6-dicarbethoxy-3-(2-(ferrocenyl)vinyl)-5-methyl-4,4-difluoro-4-bora-3a,4a-diaza-s-indacene (2) and 1,7-Diphenyl-2,6-dicarbethoxy-3,5-bis(2-(ferrocenyl)vinyl)-4,4-difluoro-4-bora-3a,4a-diaza-s-indacene (**3**).* A mixture of 1030 mg (2 mmol) of BODIPY **1**,[17] 490 mg (2.3 mmol) of ferrocenecarboxaldehyde, 500 mg (5.9 mmol) of piperidine, and 1500 mg (25 mmol) of acetic acid was refluxed in 75 mL of benzene for 3.5 h. After cooling, the solution was washed with water, dried over $Na_2SO_4$, and evaporated to dryness. The residue was chromatographed on silica gel (eluent hexane−ethyl acetate, 3:1), yielding 480 mg (34%) of monoferrocene-containing BODIPY **2** and 430 mg (27%) of diferrocene-containing BODIPY **3**. Compound **2**: mp 147−148 °C. $^1$H NMR ($CDCl_3$, 500 MHz) $\delta$ 7.70 (d, 1H, $J$ = 16.0 Hz), 7.42−7.34 (m, 7H), 7.28 (m, 4H), 6.89 (s, 1H), 4.67 (t, 2H, $J$ = 2.0 Hz), 4.52 (t, 2H, $J$ = 2.0 Hz), 4.27 (s, 5H), 4.21−4.10 (m, 4H), 2.93 (s, 3H), 1.09 (t, $J$ = 7.1 Hz, 3H), 1.06 (t, $J$ = 7.1 Hz, 3H). $^{13}$C NMR ($CDCl_3$, 125 MHz): $\delta$ 165.14, 163.94, 144.11, 132.35, 131.63, 130.08, 129.52, 128.89, 128.50, 127.78, 114.23, 81.74, 71.49, 70.07, 68.73, 61.08, 60.11, 45.36, 13.92, 13.76. Anal. Calcd for **2**, $C_{40}H_{35}BF_2FeN_2O_4$: C, 67.44; H, 4.95; N, 3.93. Found: C, 67.18; H, 4.92; N, 3.95. Compound **3**: mp 220−221 °C. $^1$H NMR ($CDCl_3$, 500 MHz) $\delta$ 7.70 (d, 2H, $J$ = 16.0 Hz), 7.44 (d, 2H, $J$ = 16.0 Hz), 7.40−7.35 (m, 6H), 7.33−7.28 (m, 4H), 6.89 (s, 1H), 4.68 (t, 4H, $J$ = 2.0 Hz), 4.50 (t, 4H, $J$ = 2.0 Hz), 4.29 (s, 10H), 4.16 (q, 4H, $J$ = 7.1 Hz), 1.06 (t, 6H, $J$ = 7.1 Hz). $^{13}$C NMR (125 MHz, $CDCl_3$) $\delta$ 165.50, 152.59, 145.12, 142.75, 135.02, 132.21, 129.67, 128.80, 128.31, 123.59, 122.24, 115.02, 82.31, 71.25, 70.12, 68.67, 61.02, 13.89. Anal. Calcd for **3**, $C_{51}H_{43}BF_2Fe_2N_2O_4$: C, 67.43; H, 4.77; N, 3.08. Found: C, 67.26; H, 4.94; N, 3.13.

*1,7-Diphenyl-2,6-dicarbethoxy-3-(2-(4-dimethylaminophenyl)-vinyl)-5-(2-(ferrocenyl)vinyl)-4,4-difluoro-4-bora-3a,4a-diaza-s-indacene (**4**).* A mixture of 142 mg (0.2 mmol) of monoferrocene BODIPY **2**, 149 mg (1 mmol) *p*-dimethyamino benzaldehyde, 42 mg (0.5 mmol) of piperidine, and 42 mg (0.7 mmol) of acetic acid was refluxed in 5 mL of toluene for 1.5 h. After cooling the solution was washed with water, dried over $Na_2SO_4$, and evaporated to dryness. The residue was chromatographed on silica gel (eluent hexane−ethyl acetate, 3:1), yielding 96 mg (57%) of compound **4**. Mp 171−172 °C. $^1$H NMR (500 MHz, $CDCl_3$) $\delta$ 7.80−7.66 (m, 3H), 7.61 (d, 2H, $J$ = 8.8 Hz), 7.46 (d, 1H, $J$ = 16.0 Hz), 7.43−7.31 (m, 10H), 6.86 (s, 1H), 6.75 (d, 2H, $J$ = 8.8 Hz), 4.73−4.68 (m, 2H), 4.54−4.49 (m, 2H), 4.32 (s, 5H), 4.24−4.16 (m, 4H), 3.09 (s, 6H), 1.13−1.07 (m, 6H). $^{13}$C NMR ($CDCl_3$, 125 MHz): $\delta$ 165.58, 165.35, 153.47, 152.15, 151.50, 145.00, 144.34, 141.71, 135.20, 134.62, 132.37, 132.09, 129.81, 129.64, 129.55, 128.66, 128.49, 128.24, 128.15, 125.05, 122.99, 122.53, 121.63,



DOI: 10.1021/acs.inorgchem.5b00992
*Inorg. Chem.* 2015, 54, 7915−7928

**Table 1. Summary of Crystallographic Data for Compounds 2−4 and 6**

| | 2 | 3 | 4 | 6 |
|---|---|---|---|---|
| empirical formula | $C_{40}H_{35}B_1F_2Fe_1N_2O_4$ | $C_{51}H_{43}B_1F_2Fe_2N_2O_4$ | $C_{49}H_{44}B_1F_2Fe_1N_3O_4$ | $C_{43}H_{38}B_1F_2Fe_1N_3O_3$ |
| fw | 712.38 | 908.41 | 843.56 | 748.94 |
| cryst syst | orthorhombic | triclinic | monoclinic | triclinic |
| space group, $Z$ | *Iba*2, 8 | *P*-1, 2 | $P2_1/n$, 4 | *P*-1, 2 |
| $a$ (Å) | 18.720(2) | 11.4501(3) | 11.2986(2) | 13.5752(2) |
| $b$ (Å) | 48.938(7) | 12.3332(3) | 11.5422(8) | 15.8246(2) |
| $c$ (Å) | 8.0507(9) | 16.1010(11) | 36.2597(6) | 18.0956(12) |
| $\alpha$ (deg) | 90.0 | 110.795(8) | 90.0 | 103.130(7) |
| $\beta$ (deg) | 90.0 | 94.810(7) | 116.998(8) | 94.420(7) |
| $\gamma$ (deg) | 90.0 | 94.587(7) | 90.0 | 91.117(6) |
| vol. (Å$^3$) | 7375.4(15) | 2103.4(2) | 4213.3(4) | 3771.7(3) |
| $\rho_{calcd}$ (g/cm$^3$) | 1.283 | 1.434 | 1.330 | 1.319 |
| $\mu$(K$\alpha$) (mm$^{-1}$) | 0.461/Mo | 0.749/Mo | 0.416/Mo | 3.644/Cu |
| $\theta_{max}$ (deg) | 23.254 | 27.449 | 27.484 | 65.077 |
| $R_{int}$ | 0.259 | 0.0350 | 0.0294 | 0.060 |
| GoF($F^2$) | 0.9932 | 0.9345 | 0.9940 | 0.9457 |
| $R_1$ ($F^2 > 2\sigma(F^2)$) | 0.1118 | 0.0438 | 0.0784 | 0.0997 |
| $wR_2$ (all data) | 0.2346 | 0.0913 | 0.1644 | 0.2496 |
| $\Delta\rho_{max}/\Delta\rho_{min}$ (e/Å$^3$) | 1.16/−0.96 | 0.71/−0.79 | 2.41/−0.79 | 1.40/−1.10 |

**Table 2. Selected Bond Lengths (Angstroms) and Angles (degrees) for D−A BODIPYs 2−4 and 6**

| | | | |
|---|---|---|---|
| **compound 2** | | | |
| Fe(1)−$C_{av}$(Cp)[a] | 2.036(18) | Fe(1)−$C_{av}$(Cp)[b] | 2.06(2) |
| C(1)−C(11) | 1.38(3) | C(11)−C(12) | 1.36(3) |
| C(12)−C(13) | 1.46(3) | N(1)−B(1) | 1.55(3) |
| N(2)−B(1) | 1.53(3) | B(1)−F(1) | 1.33(2) |
| B(1)−F(2) | 1.34(3) | C(1)−C(11)−C(12) | 123(2) |
| C(11)−C(12)−C(13) | 120(3) | N(1)−B(1)−N(2) | 106.3(19) |
| F(1)−B(1)−F(2) | 110(2) | N(1)−C(13)−C(12)−C(11) | 153.2(2) |
| C(2)−C(1)−C(11)−C(12) | 166.4(2) | | |
| **compound 3** | | | |
| Fe(1)−$C_{av}$(Cp)[a] | 2.044(3) | Fe(2)−$C_{av}$(Cp)[a] | 2.049(3) |
| Fe(1)−$C_{av}$(Cp)[b] | 2.047(3) | Fe(2)−$C_{av}$(Cp)[b] | 2.052(3) |
| C(1)−C(11) | 1.451(4) | C(41)−C(42) | 1.445(4) |
| C(11)−C(12) | 1.339(4) | C(40)−C(41) | 1.341(4) |
| C(12)−C(13) | 1.442(4) | C(30)−C(40) | 1.436(4) |
| N(1)−B(1) | 1.558(4) | N(2)−B(1) | 1.564(4) |
| B(1)−F(1) | 1.380(3) | B(1)−F(2) | 1.386(4) |
| C(1)−C(11)−C(12) | 126.0(3) | C(30)−C(40)−C(41) | 126.9(3) |
| C(11)−C(12)−C(13) | 124.4(3) | C(40)−C(41)−C(42) | 125.4(3) |
| N(1)−B(1)−N(2) | 106.8(2) | F(1)−B(1)−F(2) | 110.4(2) |
| N(1)−C(13)−C(12)−C(11) | 163.77(5) | N(2)−C(30)−C(40)−C(41) | 170.15(6) |
| C(2)−C(1)−C(11)−C(12) | 173.36(5) | C(46)−C(42)−C(41)−C(40) | 173.03(5) |
| **compound 4** | | | |
| Fe(1)−$C_{av}$(Cp)[a] | 2.040(4) | C(41)−C(42) | 1.448(4) |
| Fe(1)−$C_{av}$(Cp)[b] | 2.048(4) | C(40)−C(41) | 1.345(4) |
| C(1)−C(11) | 1.450(4) | C(30)−C(40) | 1.439(4) |
| C(11)−C(12) | 1.348(4) | N(2)−B(1) | 1.551(4) |
| C(12)−C(13) | 1.444(4) | B(1)−F(2) | 1.388(4) |
| N(1)−B(1) | 1.563(4) | C(30)−C(40)−C(41) | 125.3(3) |
| **compound 4** | | | |
| B(1)−F(1) | 1.387(4) | C(40)−C(41)−C(42) | 126.9(3) |
| C(1)−C(11)−C(12) | 125.2(3) | F(1)−B(1)−F(2) | 109.4(2) |
| C(11)−C(12)−C(13) | 124.5(3) | N(2)−C(30)−C(40)−C(41) | 169.68(4) |
| N(1)−B(1)−N(2) | 106.9(2) | C(43)−C(42)−C(41)−C(40) | 177.52(4) |
| N(1)−C(13)−C(12)−C(11) | 157.94(4) | C(44)−C(45)−N(3)−C(49) | 2.96(3) |
| C(2)−C(1)−C(11)−C(12) | 176.96(5) | | |
| **compound 6** | | | |
| Fe(1)−$C_{av}$(Cp)[a] | 2.023(10) | Fe(2)−$C_{av}$(Cp)[a] | 2.020(9) |
| Fe(1)−$C_{av}$(Cp)[b] | 2.051(9) | Fe(2)−$C_{av}$(Cp)[b] | 2.032(10) |
| C(1)−C(11) | 1.469(10) | C(55)−C(56) | 1.437(10) |
| C(11)−C(12) | 1.333(11) | C(54)−C(55) | 1.331(10) |
| C(12)−C(13) | 1.443(11) | C(44)−C(54) | 1.494(10) |
| N(1)−B(1) | 1.564(11) | N(4)−B(2) | 1.555(12) |
| N(2)−B(1) | 1.526(11) | N(5)−B(2) | 1.524(10) |
| B(1)−F(1) | 1.399(10) | B(2)−F(3) | 1.386(10) |
| B(1)−F(2) | 1.373(11) | B(2)−F(4) | 1.385(10) |
| C(31)−C(32) | 1.359(13) | C(74)−C(75) | 1.347(12) |
| C(33)−O(3) | 1.222(11) | C(76)−O(6) | 1.243(11) |
| C(1)−C(11)−C(12) | 124.8(8) | C(44)−C(54)−C(55) | 122.5(8) |
| C(11)−C(12)−C(13) | 126.5(8) | C(54)−C(55)−C(56) | 123.3(8) |
| N(1)−B(1)−N(2) | 106.9(6) | N(4)−B(2)−N(5) | 107.9(6) |
| F(1)−B(1)−F(2) | 109.5(7) | F(3)−B(2)−F(4) | 109.4(7) |
| N(1)−C(13)−C(12)−C(11) | 172.29(9) | N(4)−C(56)−C(55)−C(54) | 169.71(10) |
| C(2)−C(1)−C(11)−C(12) | 174.91(9) | C(48)−C(44)−C(54)−C(55) | 175.12(9) |

[a]Average Fe−C bond distance for substituted Cp ring. [b]Average Fe−C bond distance for unsubstituted Cp ring.

114.91, 113.06, 112.06, 82.38, 70.93, 69.92, 68.48, 61.03, 60.82, 40.24, 13.80. Anal. Calcd for **4**, $C_{49}H_{44}BF_2FeN_3O_4$: C, 69.77; H, 5.26; N, 4.98. Found: C, 69.77; H, 5.18; N, 5.00.

*2-Carbethoxy-3-(2-(ferrocenyl)vinyl)-7-(1-butyl)-1,9-diphenyl-4,4-difluoro-3a,4a,7-triaza-4-bora-cyclopenta[b]fluoren-8-on (**6**).* A mixture of 110 mg (0.2 mmol) of compound **5**,[18] 66 mg (0.3 mmol) of ferrocenecarboxaldehyde, 34 mg (0.4 mmol) of piperidine, and 36 mg (0.6 mmol) of acetic acid was refluxed in 10 mL of toluene for 1 h. After cooling the solution was washed with water, dried over $Na_2SO_4$, and evaporated to dryness. The residue was chromatographed



DOI: 10.1021/acs.inorgchem.5b00992
*Inorg. Chem.* 2015, 54, 7915−7928

on silica gel (eluent hexane−ethyl acetate, 1:1), yielding 134 mg (45%) of compound **6**. Mp 153−154 °C. $^1$H NMR (500 MHz, $CDCl_3$) $\delta$ 7.75 (d, 1H, $J$ = 16.0 Hz), 7.50 (m, 2H), 7.41−7.25 (m, 9H), 7.22 (d, 1H, $J$ = 7.5 Hz), 7.08 (s, 1H), 6.77 (d, 1H, $J$ = 7.5 Hz), 4.64 (t, 2H, $J$ = 2.9 Hz), 4.52 (t, 2H, $J$ = 2.9 Hz), 4.21 (s, 5H), 4.12 (q, 2H, $J$ = 7.1 Hz), 3.85 (t, 2H, $J$ = 7.0 Hz), 1.68−1.60 (m, 2H), 1.36−1.26 (m, 2H), 1.01 (t, 3H, $J$ = 7.1 Hz), 0.86 (t, 3H, $J$ = 7.4 Hz). $^{13}$C NMR ($CDCl_3$, 125 MHz): $\delta$ 165.05, 159.36, 151.03, 147.83, 145.81, 138.13, 131.49, 130.87, 129.53, 129.18, 128.89, 128.37, 127.97, 125.49, 114.25, 97.27, 81.64, 72.03, 70.31, 69.04, 61.25, 48.72, 31.71, 30.96, 20.02, 13.76. Anal. Calcd for **6**, $C_{43}H_{38}BF_2FeN_3O_3$: C, 68.91; H, 5.11; N, 5.61. Found: C, 68.66; H, 5.13; N, 5.63.

**DFT-PCM and TDDFT-PCM Calculations.** The starting geometries of compounds **1**−**4** and **6** were adopted from the experimental X-ray data and optimized using a hybrid B3LYP exchange-correlation functional.[19] This B3LYP exchange-correlation functional was found to result in good agreement between calculated and experimentally determined bond distances and angles in ferrocene-containing compounds.[20] Energy minima in optimized geometries were confirmed by the frequency calculations (absence of the imaginary frequencies). Solvent effects were calculated using the polarized continuum model (PCM).[21] In all calculations, DCM was used as the solvent. In PCM-TDDFT calculations, the first 30 states (BODIPYs **1**, **2**, **4**, and **6**) or 50 states (BODIPY **3**) were calculated. In all calculations, full-electron Wachter's basis set[22] was utilized for iron atoms, while all other atoms were modeled using the 6-31G(d)[23] basis set. Gaussian 09 software was used in all calculations.[24] The QMForge program was used for molecular orbital analysis.[25] In the case of dyad **4**, additional geometry optimizations and single-point and TDDFT calculations were conducted using TPSSh[26] and BP86[27] exchange-correlation functionals.

**X-ray Crystallography.** Suitable for X-ray diffraction experiments, single crystals of dyads **2**−**4** and **6** were prepared by the slow evaporation of saturated DCM/MeOH solutions. A Rigaku RAPID-II diffractometer with a graphite monochromator and Mo K$\alpha$ ($\lambda$ = 0.71073 Å) or Cu K$\alpha$ ($\lambda$ = 1.54187 Å) radiation was used for X-ray diffraction data collection. All experiments were conducted at −150 °C. Multiscan absorption correction[28] was applied to the data in all cases. The crystal structures were solved by the direct method (SIR-92)[29] and refined by full-matrix least-squares method based on $F^2$ using the Crystals for Windows programs.[30] All non-hydrogen atoms were refined anisotropically, while hydrogen atoms were refined using "riding mode" with displacement parameters bonded to a parent atom: $U_{iso}(H) = 1.2U_{eq}(C)$ ($U_{eq} = 1/3(U_{11} + U_{22} + U_{33})$).

In both crystallographically independent molecules of BODIPY **6**, the *n*-butyl group was found to be disordered over two positions by a rotation along the C−N bond. Since in one of those molecules disordered chains were close, only one set of disordered butyl groups was refined (Supporting Information Figure S1). The final refined occupancies were found to be 0.5 and 0.5, respectively. A standard set of geometrical restraints was used during the refinement. The analyses of the structures and visualization of the results were done using CAMERON software.[31] Crystal data for complexes **2**−**4** and **6** are summarized in Table 1, while selected bond distances and angles are presented in Table 2. CCDC 1059186 (**2**), 1059183 (**3**), 1059184 (**4**), and 1059185 (**6**) contain the supplementary crystallographic data for all compounds. These data can be obtained free of charge via www.ccdc.cam.ac.uk/conts/retrieving.html (or from Cambridge Crystallographic Data Centre, 12 Union Road, Cambridge CB2 1EZ, U.K.; fax: (+44) 1223-336-033 or deposit@ccdc.cam.ac.uk).

**Spectroscopy Measurements.** A Jasco-720 spectrophotometer was used to collect UV−vis data. Electrochemical cyclic voltammetry (CV) and differential pulse voltammetry (DPV) measurements were conducted using a CH Instruments electrochemical analyzer utilizing a three-electrode scheme with platinum working, auxiliary, and Ag/AgCl reference electrodes. DCM was used as solvent, and either a 0.1 M solution of tetrabutylammonium perchlorate ($TBAClO_4$) or a 0.05 M solution of tetrabutylammonium tetrakis(pentafluorophenyl)borate ($TBAB(C_6F_5)_4$) was used as electrolyte. Because of its high cost, the later electrolyte was used only for experiments on dyads **3** and **4** in order to minimize the ion-pairing effect in CV and DPV experiments. In all cases, experimental redox potentials are recorded versus a decamethylferrocene ($Cp^*_2Fe$) as an internal standard. Spectroelectrochemical experiments were conducted in DCM/0.3 M $TBAClO_4$ and DCM/0.15 M $TBAB(C_6F_5)_4$ systems using a custom-made 1 mm cell and platinum mesh working electrode. NMR spectra were recorded on a Varian INOVA instrument with a 500 MHz frequency for protons and 125 MHz for carbon. Chemical shifts are reported in parts per million (ppm) and referenced to tetramethylsilane ($Si(CH_3)_4$) as an internal standard. In all cases, final assignments of $^1$H and $^{13}$C signals were made using COSY spectra. Elemental analyses were conducted by Atlantic Microlab. Steady-state fluorescence data were collected using a Cary Eclipse fluorimeter at room temperature.

Fluorescence lifetimes were measured using time-correlated single-photon counting. Samples in a 1 cm quartz cuvette were excited with a 472 nm, 40 MHz diode laser (Driver: Picoquant PDL 800-B; Head: Picoquant LDH-P-470). Emission was directed through a double monochromator (Jobin-Yvon DH-10) and detected using an avalanche photodiode (Picoquant MPD PDM). The instrument response of the system is approximately 500 ps Gaussian, full width at half-maximum (fwhm). The fluoroescence quantum yield for **1** was measured using a Fluorolog 1680 0.2 m double spectrometer running Datamax software against Rhodimine 6G in ethanol as the external standard, $\phi$ = 0.94.[32]

Pump−probe experiments with subpicosecond time resolution were used to characterize the exited state lifetimes for samples with low emission yields or lifetimes shorter than the time resolution accessible to the single-photon counting setup. A home-built regeneratively amplified Ti:sapphire-based system generated 800 uJ pulses at 1 kHz that were centered at 810 nm and 60 fs wide.[33] The light was divided into pump and probe lines. The pump line was either frequency doubled in BBO to 405 nm or used to drive a home-built noncollinear optical parametric amplifier and provide pump light at 619 nm. The probe line, ∼20 $\mu$W, was focused into a 2 mm thick sapphire window to generate continuum (450−750 nm). The pump and probe beams were delayed with respect to each other using mechanical translation stages (Newport, UTM 150PP.1), focused, and crossed at the sample using an off-axis parabolic mirror. After the sample, the probe light was collimated and directed into a monochromator (Princton Instruments SP2150i). The spectrally dispersed probe was detected using a linear array of 256 silicon diodes (Hamamatsu, S3902-256Q). The pump beam was modulated at one-half the laser repetition rate using a mechanical chopper wheel, and the change in optical density was determined for sequential pairs of probe pulses (with and without the pump pulse). The data shown were taken using pump pulse energies of 78−88 nJ. Samples were continuously pumped through a 1 mm optical path length cell with 1 mm spectrosil windows. Samples had an optical density at the pump wavelength of 0.2 across the 1 mm cell. Absorption spectra taken of the samples before and after the pump probe experiments was identical within experimental error, providing a lack of evidence for any measurable photochemical degradation during the experiments.

## RESULTS AND DISCUSSION

**Synthesis.** The preparation of asymmetric monoferrocene derivative **2** requires a statistical condensation of ferrocenecarbaldehyde with an equimolar amount of dimethyl BODIPY **1** under standard Knoevenagel condensation conditions (Scheme 1). The statistical nature of such condensation unavoidably leads to formation of symmetric diferrocenyl BODIPY **3** along with large quantities of the starting BODIPY **1**. Fortunately, all three major reaction products can be easily separated using conventional chromatography methods. The monoferrocene-substituted BODIPY **2** can undergo a second Knoevenagel condensation with an excess of *p*-dimethylaminobenzaldehyde to form an asymmetric BOIDPY **4** in relatively high yield (Scheme 1). The pyridone BODIPY **5** can undergo a Knoevenagel condensation with ferrocenecarbaldehyde to form D−A assembly **6** in 45% yield (Scheme 1). All target


DOI: 10.1021/acs.inorgchem.5b00992
Inorg. Chem. 2015, 54, 7915−7928

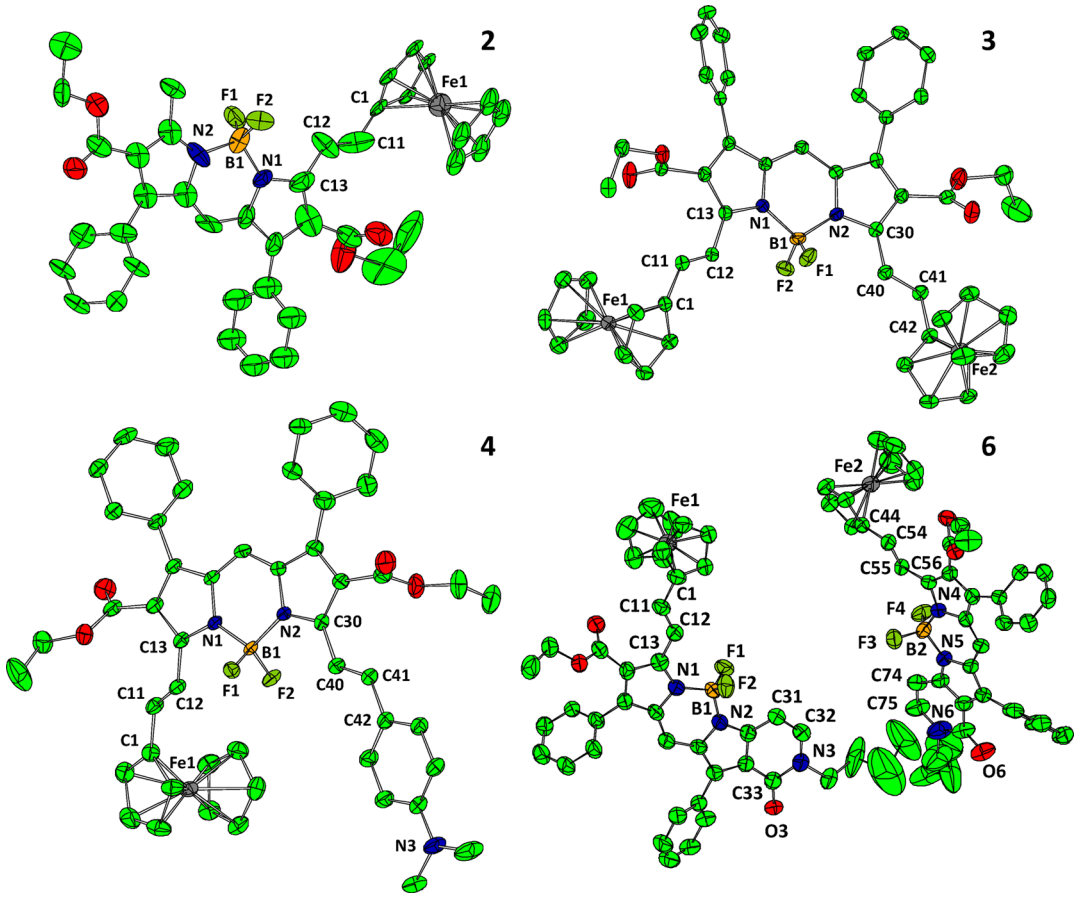


**Figure 1.** CAMERON drawing of the X-ray crystal structures of BODIPYs **2**–**4** and **6**.

compounds are surprisingly stable at ambient conditions and were purified by chromatography using silica gel. All new organometallic BODIPY compounds are soluble in a variety of organic solvents. All structures of the target compounds were confirmed by $^{1}$H, $^{13}$C, and COSY NMR, UV–vis spectroscopy, electro- and spectroelectrochemistry, as well as elemental analyses and X-ray crystallography. To the best of our knowledge, besides of the dyads **2**, **4**, and **6**, there are only two reported asymmetric ferrocene-containing BODIPYs with the organometallic groups attached to the $\alpha$ position of BODIPY via vinyl bridge.[15i,j]

**X-ray Crystal Structures.** Confirmation of the molecular structures of organometallic BODIPY dyads **2**–**4** and **6** was provided by single-crystal X-ray experiments. X-ray experimental data for BODPYs **2**–**4** and **6** are listed in Table 1, while important bond lengths and bond angles are listed in Table 2. CAMERON diagrams of ferrocene-containing BODIPYs **2**–**4** and **6** are shown in Figure 1. In agreement with all previously reported structures,[15] the BODIPY core in all complexes is planar. In all dyads, the boron atom was found in a pseudotetrahedral $N_2F_2$ environment with two longer B–N bonds and two shorter B–F bonds. N–B–N and F–B–F angles were found to be close to tetrahedral values. Bonds in the $C_{Fc}$–C═C–$C_{BODIPY}$ fragment clearly alternate with a central –C═C– bond distance being close to the typical isolated double-bond distance (~1.34 Å) and $C_{Fc}$–C═ and ═C–$C_{BODIPY}$ bond distances being close to standard Ar–C($sp^2$) values (~1.45 Å). Such bond distance alternation correlates well with an observed ~125° value for –C–C═C– angles in all target BODIPYs. Similarly, in the case of *p*-dimethylamino-phenyl BODIPY **4**, $C_{Ar}$–C═C–$C_{BODIPY}$ fragment also has an alternating bond distance and is almost coplanar with the phenyl ring $NMe_2$ group, suggesting strong conjugation into the $\pi$ system of BODIPY **4**. In contrast, phenyl groups in all studied ferrocenyl-containing BODIPYs are significantly rotated from the BODIPY $\pi$ system reducing their conjugation with the BODIPY core. Conjugation of the ferrocene substituents into the core $\pi$ system of BODIPY is also quite obvious from the values of $C_{Fc}$–$C_{Fc}$–C═C– torsion angles, which were observed between 173.03° and 176.96° (Table 2). Similar conjugation of the 4-$NMe_2$–$C_6H_4$–C═C– fragment into the BODIPY $\pi$ system was also observed in the case of dyad **4**. Indeed, the torsion C(43)–C(42)–C(41)–C(40) angle is close to 180°. Finally, in the case of pyridone-containing BODIPY **6**, both –C═C– and –C═O bonds in the pyridone fragment resemble isolated double bonds with typical bond lengths.

**Spectroscopy.** Good solubility of the target BODIPYs in common solvents aided their characterization. $^{1}$H NMR spectroscopy of BODIPYs **2**–**4** and **6** confirms the transformation of the $\alpha$-methyl fragment in the parent BODIPY **1** into a vinylferrocene group with a characteristically large spin–spin coupling constant for vinylic CH═CH protons. The presence of the ferrocene groups can be clearly seen from the Cp–H 2H:2H:5H pattern between 4 and 5 ppm. Despite the asymmetric nature of dyads **2**, **4**, and **6**, their ester group protons were observed at the same positions (Supporting Information Figures S2–S5).

UV–vis spectra of BODIPYs **2**–**4** and **6** are shown in Figure 2, and peak positions are listed in Table 3. Similar to the



DOI: 10.1021/acs.inorgchem.5b00992
*Inorg. Chem.* 2015, 54, 7915–7928

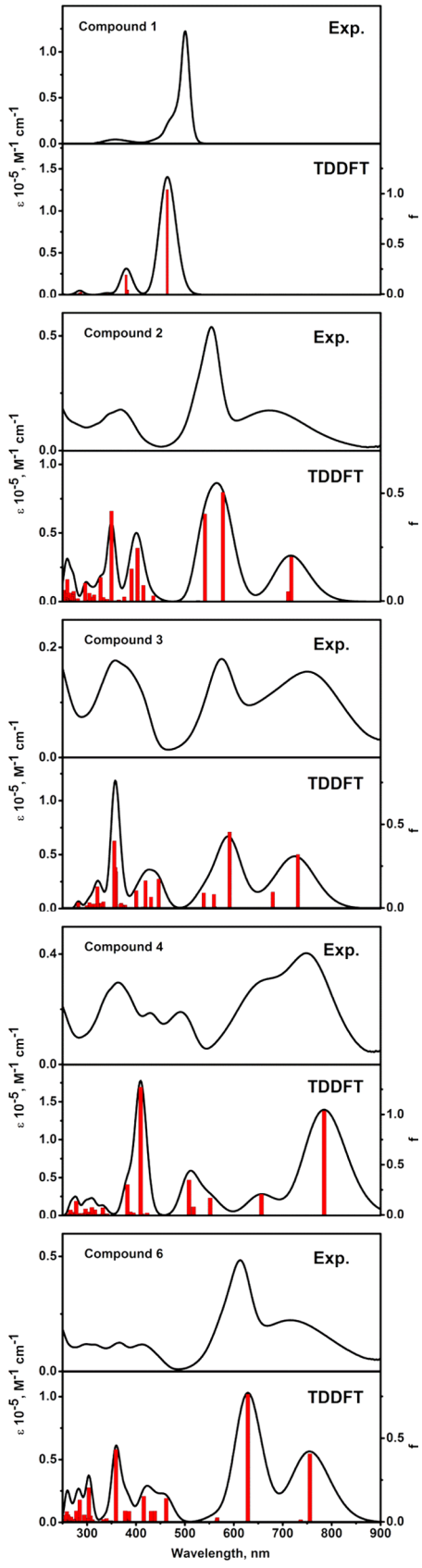


**Figure 2.** Experimental and TDDFT-predicted UV−vis spectra of BODIPYs **1**−**4** and **6** in DCM.

previously reported ferrocene−BODIPY dyads with conjugation between the substituents,[15a−e] UV−vis spectra of dyads **2**, **3**, and **6** have intense and broad low-energy bands ranging between 673 and 750 nm. More intense narrow transitions were observed between 554 and 613 nm. Since no low-energy broad bands in the NIR region were observed in the parent BODIPYs **1** and **5**, those can be tentatively assigned to the MLCT transitions, while narrow bands between 554 and 613 nm observed in dyads **2**, **3**, and **6** can be attributed to the BODIPYs $\pi \rightarrow \pi^*$ transitions. Several overlapping bands were also observed in these dyads. Low-energy as well as UV (∼360 nm) bands in diferrocenyl derivative **3** have close intensities with the $\pi \rightarrow \pi^*$ transition at 575 nm, while the similar bands in monoferrocene BODIPY **2** are about one-half of the intensity of the $\pi \rightarrow \pi^*$ transitions at 554 nm. The UV−vis spectrum of dyad **4** is quite different than BODIPYs **1**−**3**, **5**, and **6**. It has a complex NIR band with two maxima at 750 and 650 nm, and its UV−vis spectrum exhibits panchromatic behavior (Figure 2). The broad nature of the NIR band in **4** suggests several overlapping charge-transfer and $\pi \rightarrow \pi^*$ transitions.

**Table 3. UV−vis Spectra of the Target BODIPYs 2−4 and 6 in DCM**

| compound | $\lambda_{abs}$, nm ($\varepsilon \times 10^{-3}$, $M^{-1}\cdot cm^{-1}$) |
|---|---|
| **2** | 369(18), 554(54), 671(18) |
| **3** | 358(17), 575(18), 750(16) |
| **4** | 363(29), 650(31), 750(40) |
| **6** | 366(12), 613(48), 715(22) |

**Redox Properties.** The redox properties of the ferrocene−BODIPY dyads were investigated using cyclic voltammetry (CV) and differential pulse voltammetry (DPV) (Table 4 and Figure 3). Since it might be expected that the ion pairing would play an important role in generation of the mixed-valence diferrocenyl BODIPY **3** species, electrochemical and spectroelectrochemical experiments for this dyad were conducted using a noncoordinating $TBAB(C_6F_5)_4$ electrolyte.[34] All other data were collected using a standard DCM/$TBAClO_4$ system. In general, electrochemical data on ferrocene-containing dyads **2**−**4** and **6** are similar to previously reported redox properties of ferrocene−BODIPY complexes.[15] Indeed, the first reduction and the last oxidation processes are irreversible in all target BODIPYs (Figure 3). By comparison with previously studied BODIPYs, both processes were assigned as BODIPY centered. A fully reversible oxidation of the ferrocene group in monoferrocene dyads **2** and **6** can be clearly seen from CV and DPV data. In the case of diferrocene BODIPY **3**, ferrocene groups can be oxidized in a stepwise manner with 150 mV separation between the first and the second reversible oxidation waves. Such separation between the first and the second oxidation processes is similar to the redox behavior in well-

**Table 4. Redox Properties of BODIPYs in DCM[a]**

| compound | Ox3 | Ox2 | Ox1 | Red1 |
|---|---|---|---|---|
| **1**[b] | | | 0.7 (irr) | −1.24 (irr) |
| **2**[b] | | 0.56 (irr) | 0.08 | −1.19 (irr) |
| **3**[c] | 1.29 (irr) | 0.17 | 0.02 | −1.21 (irr) |
| **4**[b] | 0.72 (irr) | 0.31 | 0.06 | −1.16 (irr) |
| **4**[c] | 0.9 (irr) | 0.39 | 0.05 | −1.26 (irr) |
| **6**[b] | | 0.98 | 0.10 | −1.04 (irr) |

[a]All potentials are referenced to the $FcH/FcH^+$ couple. [b]DCM/0.1 M $TBAClO_4$ system. [c]DCM/0.05 M $TBAB(C_6F_5)_4$ system.



DOI: 10.1021/acs.inorgchem.5b00992
*Inorg. Chem.* 2015, 54, 7915−7928

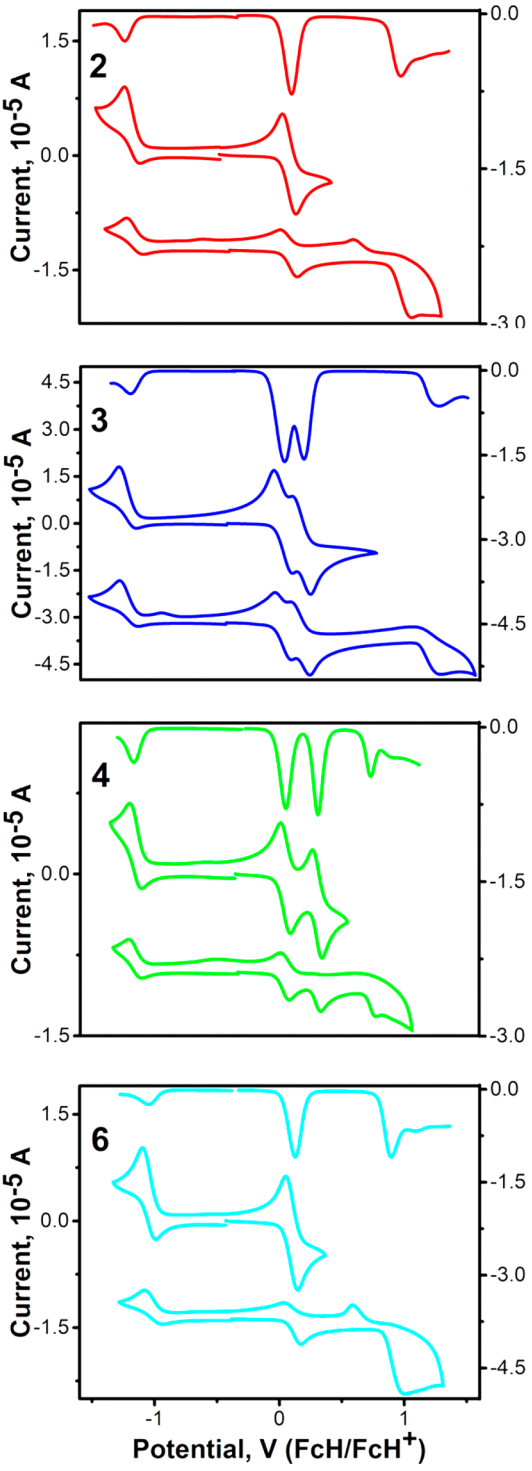


**Figure 3.** CV and DPV data for BODIPYs **2**–**4** and **6** in DCM/0.1 M $TBAClO_4$ (BODIPYs **2**, **4**, and **6**) or DCM/0.05 M $TBAB(C_6F_5)_4$ (BODIPY **3**) systems. CV data collected at 100 mV/s.

known MTFcP complexes (TFcP = 5,10,15,20-tetraferrocenylporphyrin dianion).[10c] More interestingly, two fully reversible oxidation processes were also observed in the case of BODIPY dyad **4**. Although one could be oxidation of the ferrocene and other could be oxidation of the dimethylaminophenyl fragment, it was unclear from CV and DPV data which group oxidized first. In order to minimize ion-pairing effects, additional CV and DPV data on dyad **4** were collected in DCM/$TBAB(C_6F_5)_4$ (Supporting Information Figure S6). Use of noncoordinating electrolyte did not change the reversibility of redox processes, but as expected,[33] it increased separation between the first and the second oxidation waves from 250 (DCM/$TBAClO_4$) to 340 mV (DCM/$TBAB(C_6F_5)_4$). It is interesting to note that the influence of the peripheral electron-donating or electron-withdrawing groups in BODIPYs **3**, **4**, and **6** on the oxidation potential of the ferrocene fragment is quite modest. Indeed, the first oxidation potential in BODIPYs **3** and **4** is only 30–60 mV lower than that in parent **2**, while it is 20 mV higher in BODIPY **6**.

In order to identify redox-active fragments in D–A assemblies **2**–**4** and **6** as well as obtain a spectroscopic signature of the redox-active species, we conducted spectroelectrochemical experiments on each of these systems. The results of the first reversible oxidation in BODIPYs **2** and **6** are very similar to each other (Figure 4). In both cases, during the

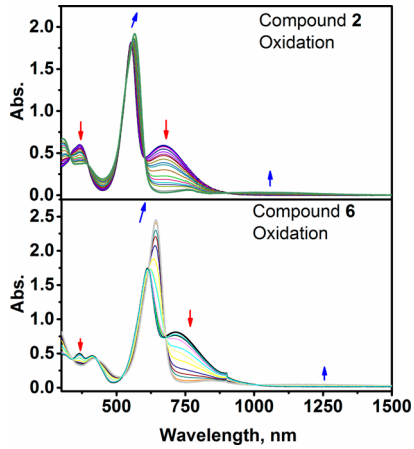


**Figure 4.** Transformation of UV–vis spectra of BODIPYs **2** and **6** during the first oxidation process recorded using an optically transparent thin-layer electrode under bulk electrolysis conditions in a spectroelectrochemical cell.

first oxidation, the low-energy MLCT band decreased in intensity, while formation of new, low-intensity bands at 754 (**2**) and 842 (**6**) nm was observed. In addition, formation of a very weak NIR band ca. 1200 nm was also observed in both systems. Finally, the most intense $\pi \rightarrow \pi^*$ transition in the visible region undergoes a red shift to 567 (**2**) and 643 (**6**) nm with increasing intensity. The $\mathbf{2}^+$ and $\mathbf{6}^+$ BODIPYs can be reduced to the corresponding neutral species (Supporting Information Figure S7). Since the only reversible oxidation is expected for ferrocene substituents in BODIPYs **2** and **6** as well as because the NIR MLCT band in these complexes undergoes the largest change while the $\pi \rightarrow \pi^*$ transition in the visible region does not change much, it is safe to propose that transformation of $\mathbf{2} \rightarrow \mathbf{2}^+$ and $\mathbf{6} \rightarrow \mathbf{6}^+$ is localized on the ferrocene fragment.

The first oxidation process in diferrocene BODIPY **3** is associated with a decrease of the low-energy MLCT band and red shift of the $\pi \rightarrow \pi^*$ transition in the visible region. A very broad IVCT band appears in the NIR region (Figure 5). During the second oxidation process, the IVCT band disappears while two new bands at 799 and 1080 nm appear in the NIR region. The final UV–vis–NIR spectrum of $\mathbf{3}^{2+}$ resembles those for $\mathbf{2}^+$ and $\mathbf{6}^+$ BODIPYs. The broad nature of the IVCT precludes any reasonable analysis of the coupling matrix elements, but its


DOI: 10.1021/acs.inorgchem.5b00992
*Inorg. Chem.* 2015, 54, 7915–7928

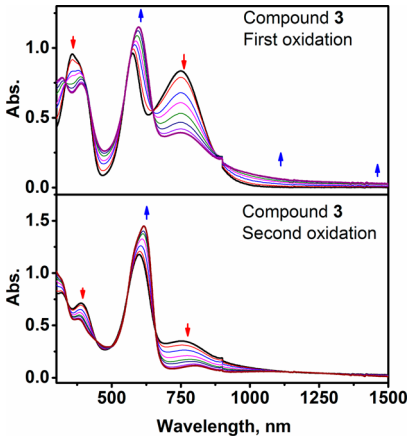


**Figure 5.** Transformation of UV−vis spectra of BODIPY **3** during the first (top) and second (bottom) oxidation processes recorded using an optically transparent thin-layer electrode under bulk electrolysis conditions in a spectroelectrochemical cell.

appearance during the first oxidation process and disappearance during the second oxidation correlate well with the mixed-valence nature of $\mathbf{3}^{+}$. Thus, spectroelectrochemical data is suggestive of the stepwise oxidation of the ferrocene substituents in BODIPY **3**. Again, $\mathbf{3}^{+}$ and $\mathbf{3}^{2+}$ cations can be easily reduced into neutral BODIPY **3** under spectroelectrochemical conditions (Supporting Information Figure S8).

During the first oxidation of monoferrocene-containing BODIPY **4** under spectroelectrochemical conditions, in both DCM/TBA$ClO_4$ and DCM/TBA$B(C_6F_5)_4$ systems the higher energy shoulder on the most intensive band at 758 nm loses intensity. The most intense band undergoes a high-energy shift and gains some intensity, while two new low-intensity NIR bands at 1000 and 1500 nm appear (Figure 6). During the

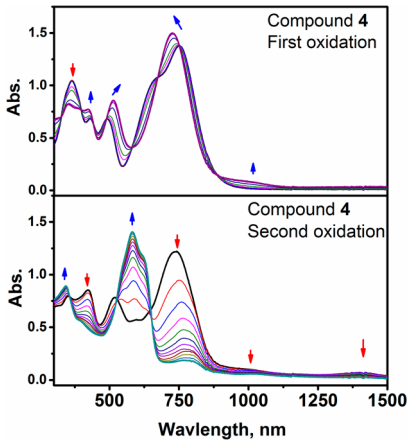


**Figure 6.** Transformation of UV−vis spectra of BODIPY **4** during the first (top) and second (bottom) oxidation processes recorded using an optically transparent thin-layer electrode under bulk electrolysis conditions in a spectroelectrochemical cell.

second oxidation, the band at 727 nm in $\mathbf{4}^{+}$ transforms into a band at 583 nm with the lower energy shoulder at 622 nm, while both low-intensity NIR bands lose their intensities. On the basis of the similarity of the NIR bands in $\mathbf{4}^{+}$ to those observed in BODIPYs $\mathbf{2}^{+}$, $\mathbf{3}^{2+}$, and $\mathbf{6}^{+}$, one can speculate that the first oxidation process in BODIPY **4** is associated with oxidation of the ferrocene group, while large changes in $\pi \rightarrow \pi^*$ transitions associated with the second oxidation process are indicative of oxidation of the *p*-dimethylaminophenyl fragment, which reduces the length of the $\pi$ system in $\mathbf{4}^{2+}$ and thus results in a high-energy shift of the main $\pi \rightarrow \pi^*$ transitions. Similar to the other BODIPYs generated at spectroelectrochemical conditions $\mathbf{4}^{+}$ and $\mathbf{4}^{2+}$ species can be reduced to the neutral BODIPY **4** (Supporting Information Figure S9).

The spectroelectrochemical data for BODIPYs **2** and **6** correlate well with their respective chemical oxidation experiments (Supporting Information Figures S10 and S11). During oxidation of BODIPYs **2** and **6** with $Fe(ClO_4)_3$, the MLCT band disappears, a high-intensity visible band undergoes a red shift, and two new weak bands in the NIR appear. Chemical titration experiments on **4**, however, are quite different from the spectroelectrochemical data (Figure 7). Both high-intensity

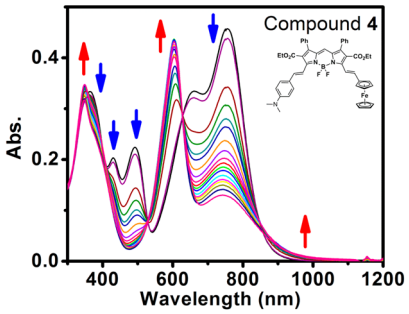


**Figure 7.** Transformation of UV−vis spectra of BODIPY **4** during its oxidation with $Fe(ClO_4)_3$.

NIR bands decrease in intensity, while two new bands at 743 and 604 nm appear in the spectrum. This transformation is close to the second oxidation step observed in spectroelectrochemical experiment and suggestive of decreased conjugation in the chromophore. Thus, one might conclude that during chemical oxidation the *p*-dimethylaminophenyl group oxidizes first. Although not completely understood, such behavior correlates well with DFT calculations presented below and can be attributed to the Lewis acidity of the $Fe^{3+}$ ion used in titrations and/or to the high concentration of TBA$ClO_4$ used in electro- and spectroelectrochemical experiments.

**Excited State Dynamics.** Similar to the other ferrocene−chromophore dyads, steady-state fluorescence in BODIPYs **2**−**4** and **6** is completely quenched as a result of electron transfer from the organometallic group to the photoexcited antennae. In contrast, the parent BODIPY **1** has a near quantitative emission yield of 0.98 ± 0.03 with an excited state lifetime of 6.13 ± 0.36 ns (single-photon counting data and fit are presented in Supporting Information Figure S12)

Transient absorption (TA) was used to measure the excited state lifetimes of **2**−**4** and **6**. The full pump−probe spectra as a function of delay time after excitation are presented in Supporting Information Figure S13. In all cases the spectra are composed of a sum of the ground state bleach (negative ΔOD) and excited state absorption (positive ΔOD). The transient spectra for **2**−**4** and **6** decayed to zero at all wavelengths probed on the time scale probed in the experiments (1 ns), and the time constants associated with excited state decay and ground state recovery were the same within experimental error. The TA data was well fitted using a single-exponential decay, Figure 8, and no evidence was found for any intermediate states in the relaxation. The conclusion was that relaxation proceeds directly to the ground electronic


DOI: 10.1021/acs.inorgchem.5b00992
*Inorg. Chem.* 2015, 54, 7915−7928

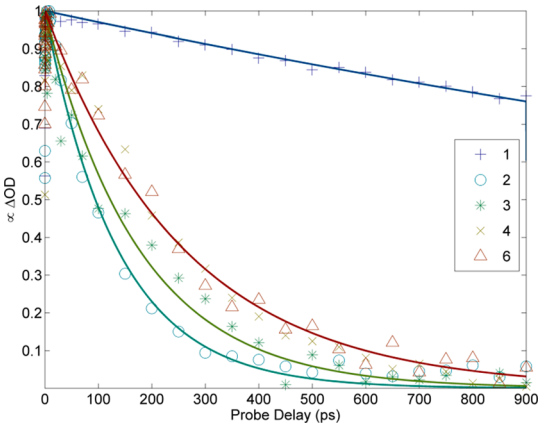


**Figure 8.** Transient absorption measured at the probe wavelengths listed in Table 5. Symbols are the data, and lines are single-exponential fits with the time constants listed in Table 5. Note that the time constant for the fits of **4** and **6** are the same within experimental error, and the two fit lines are sitting on top of each other.

state via back electron transfer to the oxidized Fc. Time constants determined by fitting the TA decay range from 136 to 260 ps and are presented in Table 5. Back electron transfer in **2**

**Table 5. Excited State Lifetimes Measured Using Transient Absorption Spectroscopy**

| compound | probe wavelength, nm | lifetime |
|---|---|---|
| **1** | 542 | 6.13 ± 0.36 ns |
| **2** | 460 | 136 ± 6 ps |
| **3** | 500 | 176 ± 15 ps |
| **4** | 543 | 260 ± 17 ps |
| **6** | 510 | 260.2 ± 9.3 ps |

and **3** is similar in rate but slightly faster for **2**, and the rates in **4** and **6** are the same within experimental error. The similar back electron-transfer rates are consistent with the fact that this homologous series maintains very similar relative energetics for the donor and acceptor levels.

The transient spectroscopy studies are clearly indicative of the usual quenching mechanism in ferrocene-containing BODIPYs, i.e., electron transfer from the low-spin iron(II) center in the ferrocene substituent to the photoexcited BODIPY core.[15,16] If this mechanism is correct then oxidation of the ferrocene group should partially restore the fluorescence of the corresponding BODIPY. Indeed, as it can be seen from Figure 9, a stepwise oxidation of the ferrocene substituents by $Fe(ClO_4)_3$ in dyads **2**–**4** and **6** results in partial fluorescence recovery. Since BODIPY dyad **4** also has a dimethylamino group, its protonation by the strong acid should also eliminate quenching of the chromophore. Indeed, titration of the dyad **4** with TFA results in an increase of the fluorescence intensity (Figure 10).

**DFT and TDDFT Calculations.** DFT-PCM and TDDFT-PCM calculations were used to gain further insights into the electronic structure, redox properties, and UV–vis spectroscopy of the new ferrocenyl-containing BODIPYs **2**–**4** and **6** as well as the reference BODIPY **1**. The B3LYP exchange-correlation functional, which allows for the prediction of spectroscopic properties and correct orbital energies of a large number of ferrocene-containing compounds,[20] was used along with DCM as a solvent in all calculations. The energy diagram

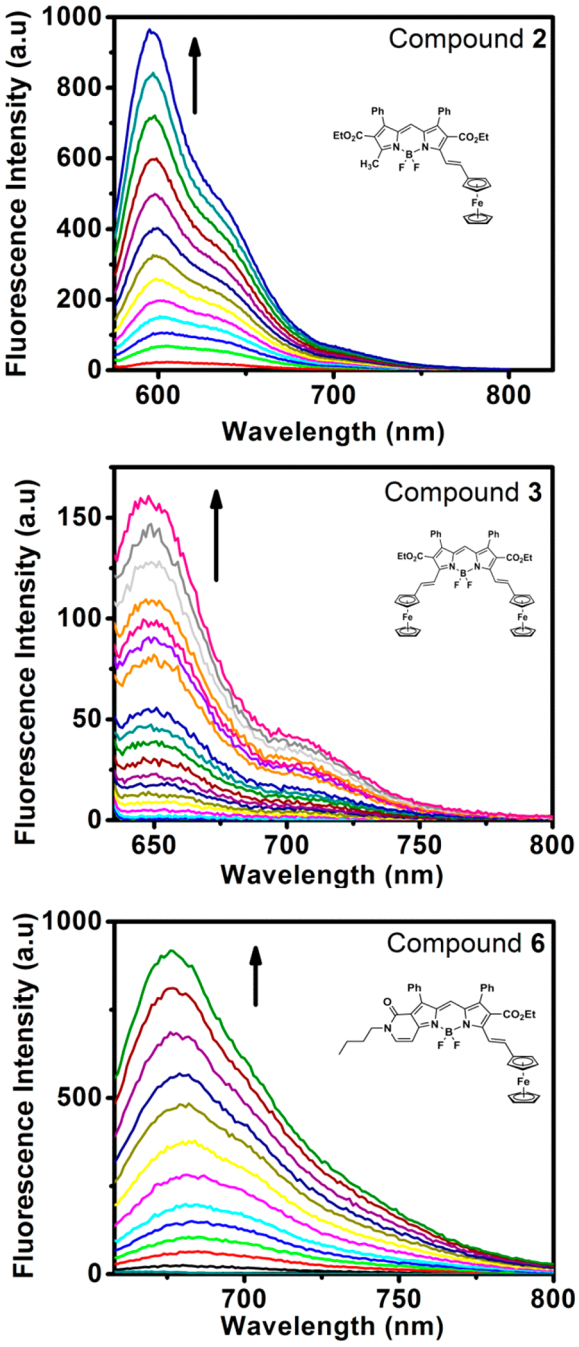


**Figure 9.** Partial fluorescence recovery upon oxidation of BODIPYs **2**, **3**, and **6** during titrations with $Fe(ClO_4)_3$.

for BODIPYs **1**–**4** and **6** calculated at the DFT-PCM level is presented in Figure 11, orbital composition analysis is shown in Table 6, and frontier orbitals of the target compounds are given in Figure 12. The HOMO–LUMO region of the reference BODIPY **1** is dominated by the $\pi$ and $\pi^*$ orbitals. The HOMO region in organometallic dyads **2**, **3**, and **6** is dominated by ferrocene-centered MOs. In particular, the ferrocene group contribution to the HOMO in these complexes varies between ~65% and 80%, while that from the BODIPY varies between ~20 and 35%. Such electronic structures suggest that the first oxidation is due to the ferrocene group in dyads **2**, **3**, and **6**, which agrees well with experimental electro- and spectroelectrochemical data. It is interesting to note that the energies of


DOI: 10.1021/acs.inorgchem.5b00992
*Inorg. Chem.* 2015, 54, 7915–7928

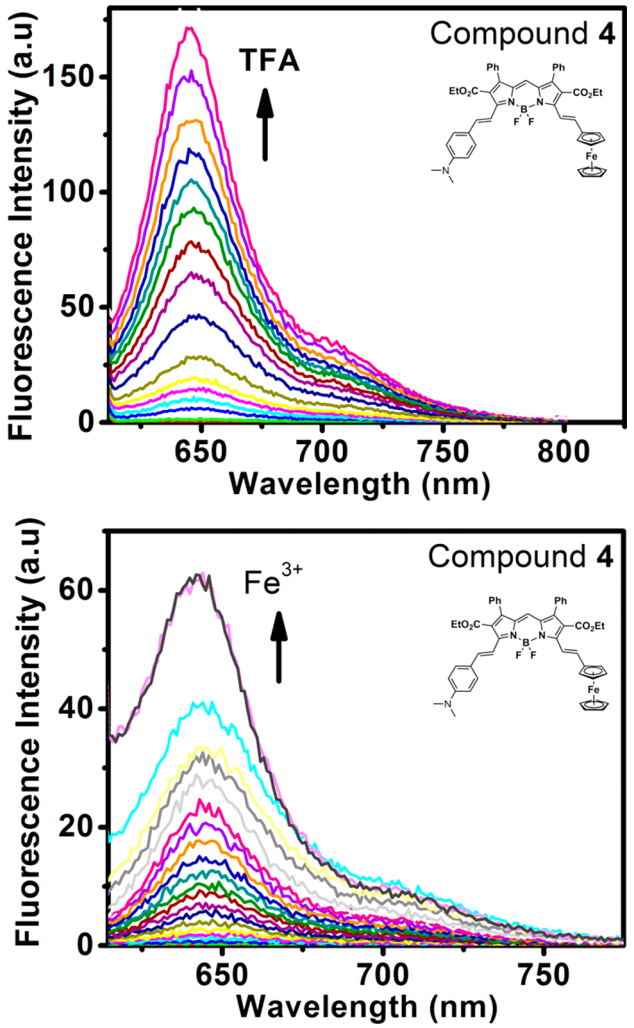


**Figure 10.** Partial fluorescence recovery upon titrations of BODIPY **4** with trifluoroacetic acid (TFA) or $Fe(ClO_4)_3$.

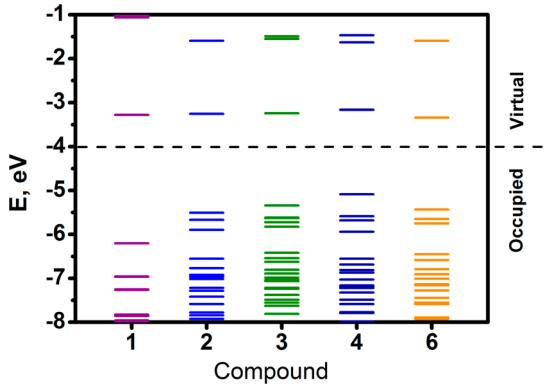


**Figure 11.** DFT-PCM-predicted molecular energy diagram for BODIPYs **1**–**4** and **6**.

the HOMO in **2** and **6** are almost identical despite the presence of an electron-withdrawing pyridone group in the latter dyad. The DFT-PCM-predicted LUMOs in dyads **2**, **3**, and **6** are ∼70–80% centered at the BODIPY core, and the LUMO is well separated in energy from the LUMO+1. The highest energy occupied $\pi$ orbital in complexes **2**, **3**, and **6** is the HOMO-5, HOMO-8, and HOMO-5, respectively. The electronic structure of these dyads suggests that the lowest energy excited states should be MLCT in nature. The electronic structure of the dimethyaminophenyl-containing dyad **4** is slightly different. Indeed, the HOMO in dyad **4** is predominantly centered at the organic part of the chromophore with ∼50% contribution from the *p*-dimethylaminophenyl fragment and only ∼14% from the ferrocene (Fe + Cp) group. The ferrocene-centered HOMO-1 is ∼0.5 eV lower in energy. The HOMO–LUMO energy gap in dyad **4** is the smallest of all ferrocene–BODIPYs discussed in this paper. Such an electronic structure of dyad **4** indicates that the first oxidation should happen at the *p*-dimethylaminophenyl fragment followed by the ferrocene group oxidation, and this disagreement will be discussed below.

In order to clarify preliminary band assignments in the UV–vis spectra of the reference BODIPY **1** as well as dyads **2**–**4** and **6** and to identify predominant MLCT transitions in these compounds, we analyzed results from TDDFT-PCM calculations. In general, TDDFT-predicted spectra are in very good agreement with experimental data (Figure 2 and Supporting Information Figure S14). In the case of reference BODIPY **1**, all intense transitions in UV–vis regions have $\pi$–$\pi^*$ nature as expected with a prominent single band observed in the visible region of the spectrum predominantly originating from the HOMO to the LUMO single electron excitation (Figure 2). In the case of the simplest ferrocenyl-containing dyad **2**, TDDFT predicts that the visible region of the UV–vis spectrum would be dominated by three key transitions (Figure 2, Supporting Information Table S1). The first excited state predicted at 718 nm correlates well with a broad band observed at 671 nm and predominantly belongs to a HOMO → LUMO single electron excitation, which has MLCT character. In addition, excited states 3 (578 nm) and 5 (541 nm) correlate well with an observed intense band at 554 nm. Excited state 3 has several major contributions with the HOMO-2 (∼24.5% of Fe) → LUMO (BODIPY $\pi^*$) contribution being the largest. The HOMO-2 → LUMO contribution also dominates in the excited state 5, which signifies its $\pi \rightarrow \pi^*$ character. According to TDDFT calculations, the NIR and visible regions of bisferrocenyl-containing BODIPY **3** should be dominated by 11 excited states with five excited states as major contributors (Supporting Information Table S1, Figure 2). The first excited state predicted at 731 nm correlates well with the experimentally observed broad band centered at 750 nm and is dominated by the HOMO (∼32% of Fe, ∼35% of Cp, and ∼33% of BODIPY) → LUMO (BODIPY $\pi^*$) single-electron transition, which has significant Fc → BODIPY ($\pi^*$) character. TDDFT also predicts a less intense band in the NIR region of dyad **3** (excited state 4, 680 nm), which has predominant MLCT character. In addition, TDDFT predicts that the band observed at 575 nm in dyad **3** includes three excited states. The first most intense excited state (excited state 5, 592 nm) has almost equivalent HOMO → LUMO and HOMO-4 → LUMO contributions. This band is further complimented by two weaker transitions predicted at 559 (excited state 7) and 539 nm (excited state 9) and both of these excited states having mixed MLCT and $\pi$–$\pi^*$ character. Since the electronic structure of dyad **6** resembles that in BODIPY **2**, it is not surprising that the TDDFT-predicted spectrum of **6** in the NIR and visible regions resembles that in dyad **2** (Figure 2, Supporting Information Table S1). Indeed, TDDFT predicts that the NIR and visible regions of BODIPY **6** should be dominated by 6 excited states with only two of those providing significant intensities. The first excited state predicted at 756


DOI: 10.1021/acs.inorgchem.5b00992
*Inorg. Chem.* 2015, 54, 7915–7928

Table 6. Compositions of the Frontier MOs of Organometallic BODIPYs 2−4 and 6 Predicted by DFT-PCM Calculations[a]

| MO | E (eV) | composition (%) Fe | $BF_2$ | N | Cp[b] | $C_{BDP}$[c] | $C_{St}$[d] |
|---|---|---|---|---|---|---|---|
| | | **2** | | | | | |
| 168 | −7.284 | 0 | 0.01 | 0.1 | 0.15 | 99.74 | |
| 169 | −7.218 | 0.11 | 0.03 | 0.18 | 0.87 | 98.82 | |
| 170 | −7.015 | 5.18 | 0.03 | 0.4 | 92.42 | 1.97 | |
| 171 | −6.962 | 0.55 | 1.22 | 14.49 | 11.4 | 72.34 | |
| 172 | −6.924 | 0.25 | 1.31 | 9.22 | 4.51 | 84.7 | |
| 173 | −6.768 | 4.52 | 0.59 | 2.95 | 43.61 | 48.33 | |
| 174 | −6.553 | 87.46 | 0.03 | 0.1 | 9.13 | 3.28 | |
| 175 | −5.897 | 24.37 | 0.08 | 0.97 | 31.3 | 43.28 | |
| 176 | −5.667 | 71.49 | 0 | 0 | 28.26 | 0.24 | |
| **177** | **−5.506** | **47.71** | **0.11** | **1.48** | **32.16** | **18.54** | |
| **178** | **−3.255** | **2.09** | **0.71** | **5.93** | **8.53** | **82.74** | |
| 179 | −1.593 | 8.59 | 0.44 | 4.08 | 33.16 | 53.73 | |
| 180 | −0.955 | 0.09 | 0.58 | 1.6 | 0.35 | 97.38 | |
| 181 | −0.707 | 3.87 | 0.46 | 6.19 | 6.94 | 82.54 | |
| 182 | −0.581 | 6.32 | 0.13 | 0.45 | 7.86 | 85.24 | |
| 183 | −0.507 | 35.16 | 0.08 | 0.18 | 46.98 | 17.61 | |
| | | **3** | | | | | |
| 218 | −6.890 | 0.1 | 2.14 | 12.55 | 0.97 | 84.24 | |
| 219 | −6.804 | 1.11 | 0.94 | 8.1 | 11.69 | 78.17 | |
| 220 | −6.622 | 80.92 | 0.04 | 0.33 | 16.85 | 1.86 | |
| 221 | −6.540 | 77.75 | 0.08 | 0.63 | 19.61 | 1.93 | |
| 222 | −6.419 | 31.17 | 0.52 | 4.46 | 53.22 | 10.62 | |
| 223 | −5.825 | 45.15 | 0.04 | 0.35 | 35.75 | 18.71 | |
| 224 | −5.723 | 71.89 | 0 | 0 | 27.92 | 0.18 | |
| 225 | −5.627 | 71.16 | 0 | 0 | 28.63 | 0.21 | |
| 226 | −5.615 | 62.18 | 0.09 | 0.85 | 32.94 | 3.94 | |
| **227** | **−5.341** | **31.99** | **0.06** | **1.35** | **35.22** | **31.39** | |
| **228** | **−3.241** | **4.09** | **0.76** | **6.36** | **18.16** | **70.63** | |
| 229 | −1.551 | 10.93 | 0.41 | 6.89 | 42.87 | 38.89 | |
| 230 | −1.492 | 7.6 | 0.28 | 1.8 | 33.15 | 57.17 | |
| 231 | −0.796 | 1.74 | 0.16 | 2.78 | 5.9 | 89.42 | |
| 232 | −0.546 | 42.02 | 0 | 0.02 | 56.84 | 1.12 | |
| 233 | −0.534 | 4.76 | 0.14 | 0.53 | 5.76 | 88.81 | |
| | | **4** | | | | | |
| 203 | −7.164 | 0.03 | 0.01 | 0.31 | 0.41 | 98.64 | 0.59 |
| 204 | −7.027 | 5.03 | 0.01 | 0.03 | 94.57 | 0.21 | 0.14 |

| MO | E (eV) | composition (%) Fe | $BF_2$ | N | Cp[b] | $C_{BDP}$[c] | $C_{St}$[d] |
|---|---|---|---|---|---|---|---|
| | | **4** | | | | | |
| 205 | −6.872 | 0.04 | 1.68 | 9.98 | 0.52 | 86.4 | 1.38 |
| 206 | −6.812 | 1.01 | 1.37 | 15.44 | 10.22 | 63.01 | 8.95 |
| 207 | −6.686 | 11.96 | 0.52 | 3.45 | 36.45 | 38 | 9.63 |
| 208 | −6.552 | 81.98 | 0.06 | 0.32 | 10.62 | 4.7 | 2.32 |
| 209 | −5.939 | 17.67 | 0.14 | 1.22 | 25.25 | 30.67 | 25.04 |
| 210 | −5.678 | 71.52 | 0 | 0 | 28.28 | 0.19 | 0 |
| 211 | −5.587 | 51.2 | 0.17 | 1.66 | 27.88 | 5 | 14.1 |
| **212** | **−5.084** | **4.66** | **0.1** | **2.36** | **9.46** | **30.67** | **52.75** |
| **213** | **−3.163** | **2.02** | **0.74** | **5.98** | **10.34** | **68.52** | **12.4** |
| 214 | −1.628 | 0.79 | 0.27 | 5.43 | 3.64 | 46.32 | 43.55 |
| 215 | −1.468 | 7.77 | 0.36 | 2.91 | 35.02 | 52.93 | 1.01 |
| 216 | −0.717 | 1.75 | 0.06 | 2.78 | 4.58 | 89.14 | 1.69 |
| 217 | −0.518 | 8.51 | 0.21 | 0.5 | 11.16 | 79.25 | 0.37 |
| 218 | −0.513 | 0.8 | 0.1 | 0.22 | 1.12 | 91.15 | 6.61 |
| | | **6** | | | | | |
| 170 | −7.157 | 1.26 | 0.06 | 1.39 | 12.57 | 84.71 | |
| 171 | −7.136 | 1.93 | 0.46 | 9.59 | 20.91 | 67.1 | |
| 172 | −7.009 | 5.21 | 0.02 | 0.15 | 93.45 | 1.17 | |
| 173 | −6.908 | 0.09 | 1.79 | 11.35 | 1.28 | 85.49 | |
| 174 | −6.794 | 0.13 | 0.82 | 6.6 | 1.25 | 91.2 | |
| 175 | −6.583 | 66.18 | 0.21 | 1.84 | 21.84 | 9.93 | |
| 176 | −6.451 | 29.81 | 0.78 | 6.46 | 30.93 | 32.01 | |
| 177 | −5.749 | 36.67 | 0.12 | 1.46 | 25.07 | 36.68 | |
| 178 | −5.650 | 70.83 | 0 | 0 | 28.93 | 0.23 | |
| **179** | **−5.432** | **33.64** | **0.07** | **1.91** | **27.16** | **37.22** | |
| **180** | **−3.340** | **1.85** | **0.51** | **5** | **7.95** | **84.69** | |
| 181 | −1.593 | 8.76 | 0.46 | 4.58 | 34.54 | 51.67 | |
| 182 | −0.922 | 0.01 | 0.22 | 0.69 | 0.34 | 98.73 | |
| 183 | −0.807 | 1.8 | 0.17 | 6.82 | 4.23 | 86.98 | |
| 184 | −0.570 | 7.01 | 0.12 | 0.38 | 8.31 | 84.19 | |
| 185 | −0.502 | 39.64 | 0.03 | 0.1 | 51.9 | 8.32 | |

[a]HOMO and LUMO are in bold font. [b]Cp = cyclopentadienyl group. [c]$C_{BDP}$ = BODIPY contribution except nitrogen and $BF_2$ groups; [d]$C_{St}$ = contribution from *N*,*N*-dimethylaminophenyl group.

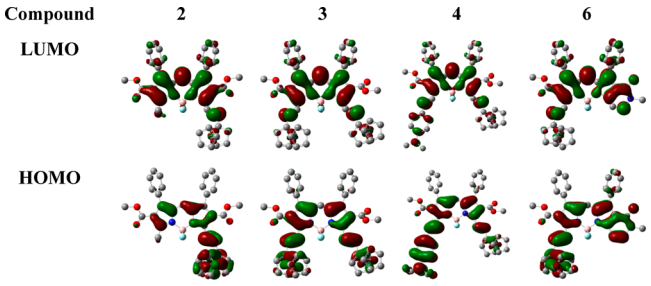


**Figure 12.** DFT-PCM-predicted frontier MOs for organometallic BODIPYs **2**−**4** and **6**.

nm is dominated by the HOMO (~34% of Fe, ~27% of Cp, and ~39% of BODIPY contributions) → LUMO (BODIPY $\pi^*$) single-electron contribution and correlates well with an experimentally observed broad band at 715 nm. This excited state has a substantial charge-transfer character. Another excited state with high intensity (excited state 3) is predicted at 629 nm and is dominated by the HOMO-4 → LUMO single-electron contribution, which is complemented by the HOMO → LUMO transition. Overall, TDDFT predicts that in the case of dyads **2**, **3**, and **6**, ferrocene-to-BODIPY charge-transfer transition(s) should be responsible for a broad low-energy NIR band observed in their experimental spectra. According to TDDFT calculations, the NIR (600−900 nm) region of the dimethylamino-containing BODIPY **4** should be dominated by two excited states (excited states 1, 785 nm, and 3, 657 nm), which predominantly consist of the HOMO → LUMO and HOMO-1 → LUMO single-electron excitations, respectively (Supporting Information Table S1 and Figure 2). The energies of both excited states correlate well with the experimental positions of two NIR bands in dyad **4** (750 and 650 nm). Since the HOMO is predominantly centered at the *p*-dimethylaminophenyl group while the LUMO is predominantly BODIPY core centered, the first excited state should have charge-transfer character, although it also can be viewed as a $\pi-\pi^*$ transition. DFT-predicted HOMO-1 composition in dyad **4** has ~51% of Fe and ~28% of Cp character, and thus, excited state 3 can be viewed as predominantly MLCT in nature. Although TDDFT calculations on dyad **4** are in very good agreement with experimental data, DFT calculations predict that the HOMO in


DOI: 10.1021/acs.inorgchem.5b00992
*Inorg. Chem.* 2015, 54, 7915−7928

this complex has $\pi$-MO nature, while the first oxidation potential value as well as spectroelectrochemical experiments on this dyad in $TBAClO_4$ and $TBAB(C_6F_5)_4$ electrolytes suggest that the first oxidation is ferrocene centered. Since the most likely reason for this discrepancy is the choice of exchange-correlation functional used in the calculation, we compared our B3LYP (20% of the Hartree−Fock exchange) calculations with those conducted using hybrid TPSSh (10% of the Hartree−Fock exchange) and pure GGA BP86 (0% of the Hartree−Fock exchange) exchange-correlation functionals (Supporting Information Figure S15). In the case of TPSSh calculations, the TDDFT- predicted UV−vis spectrum is still in a good agreement with experiment, but the predicted composition of the HOMO is suggestive of its $\pi$-MO nature similar to B3LYP calculations. On the other hand, although BP86 calculations predict that the HOMO should be almost 50% ferrocene centered, the TDDFT-predicted UV−vis spectrum of dyad **4** is in strong disagreement with experimental data. Thus, the correlation between the electronic structure, the redox properties, and the nature of the excited states in unusual BODIPY **4** should be explored in further detail, perhaps using more sophisticated computational approach.

## CONCLUSIONS

The high reactivity of the methyl groups at $\alpha$ positions of dimethyl-containing BODIPY **1** was utilized in preparation of a series of mono- (**2**, **4**, and **6**) and diferrocene (**3**) substituted donor−acceptor dyads in which organometallic substituents are fully conjugated with the BODIPY $\pi$ system. An asymmetric nature of the organometallic donor−acceptor dyads **2**, **4**, and **6** allows us to tune their photophysical and redox properties by addition of the electron-donating or electron-withdrawing groups to the peripheral position of the BODIPY core. All donor−acceptor complexes have strong absorption in the NIR region and quenched steady-state fluorescence, which can be partially restored upon oxidation of organometallic groups. X-ray crystallography of complexes **2**−**4** and **6** confirms the coplanar arrangement of ferrocene groups and BODIPY $\pi$ system. The redox properties of the target systems were studied using cyclic voltammetry (CV) and differential pulse voltammetry (DPV). In all cases, BODIPY core oxidation and reduction were found to be irreversible. It was found that the first oxidation in all dyads is ferrocene centered. The separation of redox potentials between the first and the second ferrocene-centered oxidation potentials in diferrocenyl-containing dyad **3** was ∼150 mV (DCM/0.05 M $TBAB(C_6F_5)_4$ system) despite a large Fe−Fe distance in this compound. Oxidation of the *p*-diaminophenyl fragment in BODIPY **4** was reversible and separated from the redox process at the ferrocene group by 340 mV (DCM/0.05 M $TBAB(C_6F_5)_4$ system). Density functional theory-polarized continuum model (DFT-PCM) and time-dependent (TD) DFT-PCM methods were used to probe the electronic structures as well as explain the UV−vis and redox properties of organometallic compounds **2**−**4** and **6**. DFT-PCM calculations suggest that the HOMO in dyads **2**, **3**, and **6** is ferrocene centered, while HOMO in **4** is predominantly delocalized over the BODIPY $\pi$ system. As a consequence of the electronic structure, the first oxidation in this complex is not ferrocene centered. TDDFT-PCM calculations on **4** are indicative of the $\pi \rightarrow \pi^*$ transition with lower energy than the first MLCT band, unlike the other target systems in which the MLCT transitions have lower energies. The excited state dynamics of the parent BODIPY **1** and dyads **2**−**4** and **6** were investigated using time-resolved transient spectroscopy. The results demonstrate that excited state quenching takes place via electron transfer from the ferrocene to the BODIPY, and subsequent back electron transfer to the original ground state occurs between 136 and 260 ps.

## ASSOCIATED CONTENT

### Supporting Information

Coordinates for DFT-optimized structures of **1**−**4** and **6**; predicted by TDDFT energies and expansion coefficients for BODIPYs **1**−**4** and **6**; predicted by TDDFT and experimental and UV−vis spectra of BODIPYs **1**−**4** and **6** in $cm^{-1}$ scale; TDDFT and experimental spectra of BODIPY **4** calculated at B3LYP, TPSSh, and BP86 levels; CIF for BODIPYs **2**−**4** and **6**; pump−probe spectra and time-correlated single-photon counting; $^1H$, $^{13}C$, COSY spectra of BODIPYs; CV and DPV data on **4** in DCM/0.15 M $TBAB(C_6F_5)_4$ system; reduction of $[\mathbf{2}-\mathbf{4}, \mathbf{6}]^{n+}$ under bulk electrolysis conditions; chemical oxidation of **2** and **6** with $Fe(ClO_4)_3$; positional disorder in **6**. The Supporting Information is available free of charge on the ACS Publications website at DOI: 10.1021/acs.inorgchem.5b00992.

## AUTHOR INFORMATION


### Corresponding Authors

*E-mail: kovtun@ioch.kiev.ua.
*E-mail: blank@umn.edu.
*E-mail: vnemykin@d.umn.edu.


### Notes

The authors declare no competing financial interest.

## ACKNOWLEDGMENTS

Generous support from the NSF CHE-1401375, CHE-1464711, MRI-0922366, and MRI-1420373, and Minnesota Supercomputing Institute to V.N. is greatly appreciated. This work was supported in part by a grant from NSF-DMR 1006566.

## REFERENCES


(1) (a) Melkozernov, A. N.; Barber, J.; Blankenship, R. E. *Biochemistry* **2006**, *45*, 331−345. (b) Guenes, S.; Neugebauer, H.; Sariciftci, N. S. *Chem. Rev.* **2007**, *107*, 1324−1338. (c) Sun, Y.; Welch, G. C.; Leong, W. L.; Takacs, C. J.; Bazan, G. C.; Heeger, A. J. *Nat. Mater.* **2011**, *11*, 44−48. (d) Whittell, G. R.; Hager, M. D.; Schubert, U. S.; Manners, I. *Nat. Mater.* **2011**, *10*, 176−188. (e) El-Khouly, M. E.; Fukuzumi, S.; D'Souza, F. *ChemPhysChem* **2014**, *15*, 30−47. (f) Ni, W.; Wan, X.; Li, M.; Wang, Y.; Chen, Y. *Chem. Commun.* **2015**, *51*, 4936−4950.

(2) (a) Imahori, H.; Mori, Y.; Matano, Y. *J. Photochem. Photobiol., C* **2003**, *4*, 51−83. (b) Imahori, H.; Tamaki, K.; Araki, Y.; Sekiguchi, Y.; Ito, O.; Sakata, Y.; Fukuzumi, S. *J. Am. Chem. Soc.* **2002**, *124*, 5165−5174. (c) D'Souza, F.; Chitta, R.; Gadde, S.; Islam, D.-M. S.; Schumacher, A. L.; Zandler, M. E.; Araki, Y.; Ito, O. *J. Phys. Chem. B* **2006**, *110*, 25240−25250. (d) Springer, J.; Kodis, G.; De La Garza, L.; Moore, A. L.; Moore, T. A.; Gust, D. *J. Phys. Chem. A* **2003**, *107*, 3567−3575. (e) González-Rodríguez, D.; Bottari, G. *J. Porphyrins Phthalocyanines* **2009**, *13*, 624−636. (f) Zhao, Z.; Cammidge, A. N.; Cook, M. J. *Chem. Commun.* **2009**, 7530−7532.

(3) (a) In *Molecular Mechanisms of Photosynthesis*; Blankenship, R. E., Ed.; Blackwell Science: Malden, MA, 2002. (b) Aratani, N.; Osuka, A. In *Handbook of Porphyrin Science*; Kadish, K. M., Smith, K. M., Guilard, R., Eds.; World Scientific Publishing Co. Pte. Ltd.: Singapore, 2010; Vol. *1*, pp 1−132. (c) Balaban, T. S. In *Handbook of Porphyrin Science*; Kadish, K. M., Smith, K. M., Guilard, R., Eds.; World Scientific Publishing Co. Pte. Ltd. 2010; Vol. *1*, pp 221−306. (d) Yoon, Z. S.; Yang, J.; Yoo, H.; Cho, S.; Kim, D. In *Handbook of Porphyrin Science*;




DOI: 10.1021/acs.inorgchem.5b00992
*Inorg. Chem.* 2015, 54, 7915−7928

Kadish, K. M., Smith, K. M., Guilard, R., Eds.; World Scientific Publishing Co. Pte. Ltd.: Singapore, 2010; Vol. *1*, pp 439−506.
(4) (a) Gonzalez-Rodriguez, D.; Carbonell, E.; Rojas, G. M.; Castellanos, C. A.; Guldi, D. M.; Torres, T. *J. Am. Chem. Soc.* **2010**, *132*, 16488−16500. (b) El-Khouly, M. E.; Shim, S. H.; Araki, Y.; Ito, O.; Kay, K.-Y. *J. Phys. Chem. B* **2008**, *112*, 3910−3917. (c) Ziessel, R.; Ulrich, G.; Elliott, K. J.; Harriman, A. *Chem.—Eur. J.* **2009**, *15*, 4980−4984. (d) Mauldin, C. E.; Piliego, C.; Poulsen, D.; Unruh, D. A.; Woo, C.; Ma, B.; Mynar, J. L.; Frechet, J. M. J. *ACS Appl. Mater. Interfaces* **2010**, *2*, 2833−2838. (e) Gonzalez-Rodriguez, D.; Torres, T.; Olmstead, M. M.; Rivera, J.; Angeles Herranz, M.; Echegoyen, L.; Atienza Castellanos, C.; Guldi, D. M. *J. Am. Chem. Soc.* **2006**, *128*, 10680−10681.
(5) (a) D'Souza, F.; Ito, O. In *Handbook of Porphyrin Science*; Kadish, K. M., Smith, K. M., Guilard, R., Eds.; World Scientific Publishing Co. Pte. Ltd.: Singapore, 2010; Vol. *1*, pp 307−438. (b) El-Khouly, M. E.; Ito, O.; Smith, P. M.; D'Souza, F. *J. Photochem. Photobiol., C* **2004**, *5*, 79−104. (c) Fukuzumi, S. *Phys. Chem. Chem. Phys.* **2008**, *10*, 2283−2297. (d) D'Souza, F.; Ito, O. In *Organic Electronics and Photonics*; Nalwa, H. R., Ed.; American Scientific Publishers: Stevenson Ranch, CA, 2008; Vol. *1*, Chapter 13. (e) Ohkubo, K.; Fukuzumi, S. *Bull. Chem. Soc. Jpn.* **2009**, *82*, 303−315. (f) Ohkubo, K.; Kotani, H.; Shao, J.; Ou, Z.; Kadish, K. M.; Li, G.; Pandey, R. K.; Fujitsuka, M.; Ito, O.; Imahori, H.; Fukuzumi, S. *Angew. Chem., Int. Ed.* **2004**, *43*, 853−856.
(6) (a) Su, M.; Li, Q.; Wang, Y.; Chen, S.; Zhao, H.; Bian, Z. *Youji Huaxue* **2013**, *33*, 815. (b) Loim, N. M.; Abramova, N. V.; Sokolov, V. I. *Mendeleev Commun.* **1996**, *6*, 46. (c) Burrell, A. K.; Campbell, W. M.; Jameson, G. B.; Officer, D. L.; Boyd, P. D. W.; Zhao, Z.; Cocks, P. A.; Gordon, K. C. *Chem. Commun.* **1999**, 637. (d) Narayanan, S. J.; Venkatraman, S.; Dey, S. R.; Sridevi, B.; Anand, V. R. G.; Chandrashekar, T. K. *Synlett* **2000**, 1834−1836. (e) Rhee, S. W.; Na, Y. H.; Do, Y.; Kim, J. *Inorg. Chim. Acta* **2000**, *309*, 49. (f) Shoji, O.; Okada, S.; Satake, A.; Kobuke, Y. *J. Am. Chem. Soc.* **2005**, *127*, 2201. (g) Shoji, O.; Tanaka, H.; Kawai, T.; Kobuke, Y. *J. Am. Chem. Soc.* **2005**, *127*, 8598. (h) Dammer, S. J.; Solntsev, P. V.; Sabin, J. R.; Nemykin, V. N. *Inorg. Chem.* **2013**, *52*, 9496. (i) Kubo, M.; Mori, Y.; Otani, M.; Murakami, M.; Ishibashi, Y.; Yasuda, M.; Hosomizu, K.; Miyasaka, H.; Imahori, H.; Nakashima, S. *J. Phys. Chem. A* **2007**, *111*, 5136. (j) Nemykin, V. N.; Barrett, C. D.; Hadt, R. G.; Subbotin, R. I.; Maximov, A. Y.; Polshin, E. V.; Koposov, A. Y. *Dalton Trans.* **2007**, 3378. (k) Rochford, J.; Rooney, A. D.; Pryce, M. T. *Inorg. Chem.* **2007**, *46*, 7247. (l) Nemykin, V. N.; Galloni, P.; Floris, B.; Barrett, C. D.; Hadt, R. G.; Subbotin, R. I.; Marrani, A. G.; Zanoni, R.; Loim, N. M. *Dalton Trans.* **2008**, 4233. (m) Nemykin, V. N.; Rohde, G. T.; Barrett, C. D.; Hadt, R. G.; Bizzarri, C.; Galloni, P.; Floris, B.; Nowik, I.; Herber, R. H.; Marrani, A. G.; Zanoni, R.; Loim, N. M. *J. Am. Chem. Soc.* **2009**, *131*, 14969. (n) Galloni, P.; Floris, B.; De Cola, L.; Cecchetto, E.; Williams, R. M. *J. Phys. Chem. C* **2007**, *111*, 1517. (o) Nemykin, V. N.; Rohde, G. T.; Barrett, C. D.; Hadt, R. G.; Sabin, J. R.; Reina, G.; Galloni, P.; Floris, B. *Inorg. Chem.* **2010**, *49*, 7497. (p) Rohde, G. T.; Sabin, J. R.; Barrett, C. D.; Nemykin, V. N. *New J. Chem.* **2011**, *35*, 1440. (q) Solntsev, P. V.; Neisen, B. D.; Sabin, J. R.; Gerasimchuk, N. N.; Nemykin, V. N. *J. Porphyrins Phthalocyanines* **2011**, *15*, 612.
(7) (a) Sharma, R.; Gautam, P.; Mobin, S. M.; Misra, R. *Dalton Trans.* **2013**, *42*, 5539. (b) Pareek, Y.; Ravikanth, M. *J. Organomet. Chem.* **2013**, *724*, 67. (c) Samanta, S.; Mittra, K.; Sengupta, K.; Chatterjee, S.; Dey, A. *Inorg. Chem.* **2013**, *52*, 1443. (d) Devillers, C. H.; Milet, A.; Moutet, J.-C.; Pecaut, J.; Royal, G.; Saint-Aman, E.; Bucher, C. *Dalton Trans.* **2013**, *42*, 1196. (e) Osipova, E. Y.; Rodionov, A. N.; Simenel, A. A.; Belousov, Y. A.; Nikitin, O. M.; Kachala, V. V. *J. Porphyrins Phthalocyanines* **2012**, *16*, 1225. (f) Nemykin, V. N.; Chen, P.; Solntsev, P. V.; Purchel, A. A.; Kadish, K. M. *J. Porphyrins Phthalocyanines* **2012**, *16*, 793. (g) Bakar, M. A.; Sergeeva, N. N.; Juillard, T.; Senge, M. O. *Organometallics* **2011**, *30*, 3225. (h) Lyons, D. M.; Mohanraj, J.; Accorsi, G.; Armaroli, N.; Boyd, P. D. W. *New J. Chem.* **2011**, *35*, 632. (i) Subbaiyan, N. K.; Wijesinghe, C. A.; D'Souza, F. *J. Am. Chem. Soc.* **2009**, *131*, 14646. (j) Vecchi, A.; Erickson, N. R.; Sabin, J. R.; Floris, B.; Conte, V.; Venanzi, M.; Galloni, P.; Nemykin, V. N. *Chem.—Eur. J.* **2015**, *21*, 269−279.
(8) (a) Burrell, A. K.; Campbell, W.; Officer, D. L. *Tetrahedron Lett.* **1997**, *38*, 1249. (b) Burrell, A. K.; Campbell, W. M.; Officer, D. L.; Scott, S. M.; Gordon, K. C.; McDonald, M. R. *J. Chem. Soc., Dalton Trans.* **1999**, 3349. (c) Jiao, L.; Courtney, B. H.; Fronczek, F. R.; Smith, K. M. *Tetrahedron Lett.* **2006**, *47*, 501. (d) Wang, H. J. H.; Jaquinod, L.; Olmstead, M. M.; Vicente, M. G. H.; Kadish, K. M.; Ou, Z.; Smith, K. M. *Inorg. Chem.* **2007**, *46*, 2898. (e) Gryko, D. T.; Zhao, F.; Yasseri, A. A.; Roth, K. M.; Bocian, D. F.; Kuhr, W. G.; Lindsey, J. S. *J. Org. Chem.* **2000**, *65*, 7356. (f) Schmidt, E. S.; Calderwood, T. S.; Bruice, T. C. *Inorg. Chem.* **1986**, *25*, 3718. (g) Cheng, K.-L.; Li, H.-W.; Ng, D. K. P. *J. Organomet. Chem.* **2004**, *689*, 1593. (h) Giasson, R.; Lee, E. J.; Zbao, X.; Wrighton, M. S. *J. Phys. Chem.* **1993**, *97*, 2596. (i) Muraoka, T.; Kinbara, K.; Aida, T. *Nature* **2006**, *440*, 512.
(9) (a) Maiya, G. B.; Barbe, J. M.; Kadish, K. M. *Inorg. Chem.* **1989**, *28*, 2524. (b) Solntsev, P. V.; Sabin, J. R.; Dammer, S. J.; Gerasimchuk, N. N.; Nemykin, V. N. *Chem. Commun.* **2010**, *46*, 6581. (c) Kadish, K. M.; Xu, Q. Y.; Barbe, J. M. *Inorg. Chem.* **1987**, *26*, 2565. (d) Xu, Q. Y.; Barbe, J. M.; Kadish, K. M. *Inorg. Chem.* **1988**, *27*, 2373.
(10) (a) Vecchi, A.; Galloni, P.; Floris, B.; Nemykin, V. N. *J. Porphyrins Phthalocyanines* **2013**, *17*, 165. (b) Suijkerbuijk, B. M. J. M.; Gebbink, R. J. M. K. *Angew. Chem.* **2008**, *120*, 7506;(d) *Angew. Chem., Int. Ed.* **2008**, *47*, 7396. (c) Vecchi, A.; Galloni, P.; Floris, B.; Dudkin, S. V.; Nemykin, V. N. *Coord. Chem. Rev.* **2015**, *291*, 95−171.
(11) (a) Nemykin, V. N.; Kobayashi, N. *Chem. Commun.* **2001**, 165. (b) Lukyanets, E. A.; Nemykin, V. N. *J. Porphyrins Phthalocyanines* **2010**, *14*, 1. (c) Sun, L.; Wang, S.; Tian, H. *Chem. Lett.* **2007**, *36*, 250. (d) Nemykin, V. N.; Makarova, E. A.; Erickson, N. R.; Solntsev, P. V. *Turk. J. Chem.* **2014**, *38*, 1027−1045. (e) Nemykin, V. N.; Makarova, E. A.; Grosland, J. O.; Dudkin, S. V.; Dennison, R.; Purchel, A. A. *J. Porphyrins Phthalocyanines* **2014**, *18*, 792−803.
(12) (a) Jin, Z.; Nolan, K.; McArthur, C. R.; Lever, A. B. P.; Leznoff, C. C. *J. Organomet. Chem.* **1994**, *468*, 205. (b) Poon, K.-W.; Yan, Y.; Li, X. Y.; Ng, D. K. P. *Organometallics* **1999**, *18*, 3528. (c) An, M.; Kim, S.; Hong, J.-D. *Bull. Korean Chem. Soc.* **2010**, *31*, 3272. (d) Gonzalez-Cabello, A.; Claessens, C. G.; Martin-Fuch, G.; Ledoux-Rack, I.; Vazquez, P.; Zyss, J.; Agulla-Lopez, F.; Torres, T. *Synth. Met.* **2003**, *137*, 1487. (e) Meroglu, I.; Arslan, T.; Biyiklioglu, Z.; Tosun, G. *J. Organomet. Chem.* **2014**, *749*, 261. (f) Nemykin, V. N.; Purchel, A. A.; Spaeth, A. D.; Barybin, M. V. *Inorg. Chem.* **2013**, *52*, 11004. (g) Lau, J. T. F.; Jiang, X.-J.; Ng, D. K. P.; Lo, P.-C. *Chem. Commun.* **2013**, *49*, 4274. (h) Salan, U.; Altindal, A.; Bulut, M.; Bekaroglu, O. *J. Porphyrins Phthalocyanines* **2006**, *10*, 1263.
(13) (a) Pomarico, G.; Vecchi, A.; Mandoj, F.; Bortolini, O.; Cicero, D. O.; Galloni, P.; Paolesse, R. *Chem. Commun.* **2014**, *50*, 4076. (b) Gryko, D. T.; Piechowska, J.; Jaworski, J. S.; Galezowski, M.; Tasior, M.; Cembor, M.; Butenschoen, H. *New J. Chem.* **2007**, *31*, 1613.
(14) (a) Solntsev, P. V.; Spurgin, K. L.; Sabin, J. R.; Heikal, A. A.; Nemykin, V. N. *Inorg. Chem.* **2012**, *51*, 6537−6547. (b) Verreet, B.; Rand, B. P.; Cheyns, D.; Hadipour, A.; Aernouts, T.; Heremans, P.; Medina, A.; Claessens, C. G.; Torres, T. *Adv. Energy Mater.* **2011**, *1*, 565−568. (c) Gonzalez-Rodriguez, D.; Carbonell, E.; Guldi, D. M.; Torres, T. *Angew. Chem., Int. Ed.* **2009**, *48*, 8032−8036. (d) Claessens, C. G.; Torres, T. *Chem. Commun.* **2004**, 1298−1299. (e) Rahman, G. M. A.; Lueders, D.; Rodriguez-Morgade, M. S.; Caballero, E.; Torres, T.; Guldi, D. M. *ChemSusChem* **2009**, *2*, 330−335. (f) Maligaspe, E.; Hauwiller, M. R.; Zatsikha, Y. V.; Hinke, J. A.; Solntsev, P. V.; Blank, D. A.; Nemykin, V. N. *Inorg. Chem.* **2014**, *53*, 9336−9347.
(15) (a) Galangau, O.; Fabre-Francke, I.; Munteanu, S.; Dumas-Verdes, C.; Clavier, G.; Meallet-Renault, R.; Pansu, R. B.; Hartl, F.; Miomandre, F. *Electrochim. Acta* **2013**, *87*, 809. (b) Khan, T. K.; Pissurlenkar, R. R.S.; Shaikh, M. S.; Ravikanth, M. *J. Organomet. Chem.* **2012**, *697*, 65−73. (c) Misra, R.; Dhokale, B.; Jadhav, T.; Mobin, S. M. *Dalton Trnas.* **2013**, *42*, 13658−13666. (d) Pena-Cabrera, E.; Aguilar-Aguilar, A.; Gonzalez-Domingues, M.; Lager, E.; Zamudio-Vazquez, R.; Godoy-Vargas, J.; Villanueva-Garcia, F. *Org. Lett.* **2007**, *9*, 3985−3988. (e) Yin, X.; Li, Y.; Li, Y.; Zhu, Y.; Tang, X.; Zheng, H.; Zhu, D.


DOI: 10.1021/acs.inorgchem.5b00992
*Inorg. Chem.* 2015, 54, 7915−7928

*Tetrahedron* **2009**, *65*, 8373−8377. (f) Gautam, P.; Dhokale, B.; Mobin, S. M.; Misra, R. *RSC Adv.* **2012**, *2*, 12105−12107. (g) Misra, R.; Dhokale, B.; Jadhav, T.; Mobin, S. M. *Organometallics* **2014**, *33*, 1867−1877. (h) Yin, X.; Li, Y.; Zhu, Y.; Jing, X.; Li, Y.; Zhu, D. *Dalton Trans.* **2010**, *39*, 9929−9935. (i) Ziessel, R.; Retailleau, P.; Elliott, K. J.; Harriman, A. *Chem.—Eur. J.* **2009**, *15*, 10369−10374. (j) Liu, J.-Y.; El-Khouly, M. E.; Fukuzumi, S.; Ng, D. K. P. *ChemPhysChem* **2012**, *13*, 2030−2036.

(16) (a) Ziegler, C. J.; Chanawanno, K.; Hasheminsasab, A.; Zatsikha, Y. V.; Maligaspe, E.; Nemykin, V. N. *Inorg. Chem.* **2014**, *53*, 4751. (b) Amin, A. N.; El-Khouly, M. E.; Subbaiyan, N. K.; Zandler, M. E.; Supur, M.; Fukuzumi, S.; D'Souza, F. *J. Phys. Chem. A* **2011**, *115*, 9810−9819. (c) Bandi, V.; El-Khouly, M. E.; Ohkubo, K.; Nesterov, V. N.; Zandler, M. E.; Fukuzumi, S.; D'Souza, F. *Chem.—Eur. J.* **2013**, *19*, 7221−7230. (d) Bandi, V.; El-Khouly, M. E.; Ohkubo, K.; Nesterov, V. N.; Zandler, M. E.; Fukuzumi, S.; D'Souza, F. *J. Phys. Chem. C* **2014**, *118*, 2321−2332. (e) Maligaspe, E.; Pundsack, T. J.; Albert, L. M.; Zatsikha, Y. V.; Solntsev, P. V.; Blank, D. A.; Nemykin, V. N. *Inorg. Chem.* **2015**, *54*, 4167−4174.

(17) Shandura, M. P.; Yakubovskyi, V. P.; Kovtun, Y. P. *J. Heterocycl. Chem.* **2009**, *46*, 1386−1391.

(18) Zatsikha, Y. V.; Yakubovskyi, V. P.; Shandura, M. P.; Dubey, I. Y.; Kovtun, Y. P. *Tetrahedron* **2013**, *69*, 2233−2238.

(19) (a) Becke, A. D. *J. Chem. Phys.* **1993**, *98*, 5648−5652. (b) Lee, C.; Yang, W.; Parr, R. G. *Phys. Rev. B: Condens. Matter Mater. Phys.* **1988**, *37*, 785−789.

(20) (a) Firme, C. L.; Pontes, D.; de, L.; Antunes, O. A. C. *Chem. Phys. Lett.* **2010**, *499*, 193−198. (b) Kalamse, V.; Wadnerkar, N.; Chaudhari, A. *J. Phys. Chem. C* **2010**, *114*, 4704−4709. (c) Meylemans, H. A.; Damrauer, N. H. *Inorg. Chem.* **2009**, *48*, 11161−11175. (d) Alparone, A.; Reis, H.; Papadopoulos, M. G. *J. Phys. Chem. A* **2006**, *110*, 5909−5918. (e) Solntsev, P. V.; Dudkin, S. V.; Sabin, J. R.; Nemykin, V. N. *Organometallics* **2011**, *30*, 3037−3046. (f) Goetsch, W. R.; Solntsev, P. V.; Van Stappen, C.; Purchel, A. A.; Dudkin, S. V.; Nemykin, V. N. *Organometallics* **2014**, *33*, 145−157.

(21) Tomasi, J.; Mennucci, B.; Cammi, R. *Chem. Rev.* **2005**, *105*, 2999−3093.

(22) Wachters, A. J. H. *J. Chem. Phys.* **1970**, *52*, 1033−1036.

(23) McLean, A. D.; Chandler, G. S. *J. Chem. Phys.* **1980**, *72*, 5639−5648.

(24) Frisch, M. J.; Trucks, G. W.; Schlegel, H. B.; Scuseria, G. E.; et al. *Gaussian 09*, Revision D.1; Gaussian, Inc.: Wallingford, CT, 2009. For full citation, see Supporting Information.

(25) Tenderholt, A. L. *QMForge*, Version 2.1; Stanford University: Stanford, CA.

(26) Tao, J. M.; Perdew, J. P.; Staroverov, V. N.; Scuseria, G. E. *Phys. Rev. Lett.* **2003**, *91*, 146401.

(27) (a) Becke, A. D. *Phys. Rev. A: At., Mol., Opt. Phys.* **1988**, *38*, 3098−3100. (b) Perdew, J. P. *Phys. Rev. B: Condens. Matter Mater. Phys.* **1986**, *33*, 8822−8824.

(28) Otwinowski, Z.; Minor, W. In *Methods in Enzymology*; Carter, C. W., Jr., Sweet, R. M., Eds.; Academic Press: New York, 1997; Vol. *276*, pp 307—326.

(29) Altomare, A.; Cascarano, G.; Giacovazzo, C.; Guagliardi, A.; Burla, M. C.; Polidori, G.; Camalli, M. *J. Appl. Crystallogr.* **1994**, *27*, 435.

(30) Betteridge, P. W.; Carruthers, J. R.; Cooper, R. I.; Prout, K.; Watkin, D. J. *J. Appl. Crystallogr.* **2003**, *36*, 1487.

(31) Watkin, D. J.; Prout, C. K.; Pearce, L. J. *CAMERON*; Chemical Crystallography Laboratory, University of Oxford: Oxford, U.K., 1996.

(32) Fischer, M.; Georges, J. *Chem. Phys. Lett.* **1996**, *260*, 115−118.

(33) Underwood, D. F.; Blank, D. A. *J. Phys. Chem. A* **2003**, *107*, 956−961.

(34) (a) Barrire, F.; Geiger, W. E. *J. Am. Chem. Soc.* **2006**, *128*, 3980. (b) Poppitz, E. A.; Hildebrandt, A.; Korb, M.; Lang, H. *J. Organomet. Chem.* **2014**, *752*, 133.



DOI: 10.1021/acs.inorgchem.5b00992
*Inorg. Chem.* 2015, 54, 7915−7928